High-Resolution Observations of a Destructive Macroburst®

SAMUEL J. CHILDS, a RUSS S. SCHUMACHER, AND REBECCA D. ADAMS-SELIN

^a Department of Atmospheric Science, Colorado State University, Fort Collins, Colorado ^b Atmospheric and Environmental Research, Inc., Bellevue, Nebraska

(Manuscript received 16 December 2020, in final form 1 June 2021)

ABSTRACT: Shortly after 0600 UTC (midnight MDT) 9 June 2020, a rapidly intensifying and elongating convective system produced a macroburst and extensive damage in the town of Akron on Colorado's eastern plains. Instantaneous winds were measured as high as 51.12 m s⁻¹ at 2.3 m AGL from an eddy covariance (EC) tower, and a 50.45 m s⁻¹ wind gust from an adjacent 10-m tower became the highest official thunderstorm wind gust ever measured in Colorado. Synoptic-scale storm motion was southerly, but surface winds were northerly in a postfrontal air mass, creating strong vertical wind shear. Extremely high-resolution temporal and spatial observations allow for a unique look at pressure and temperature tendencies accompanying the macroburst and reveal intriguing wave structures in the outflow. At 10-Hz frequency, the EC tower recorded a 5-hPa pressure surge in 19 s immediately following the strongest winds, and a 15-hPa pressure drop in the following 3 min. Surface temperature also rose 1.5°C in less than 1 min, concurrent with the maximum wind gusts, and then fell sharply by 3.5°C in the following minute. Shifting wind direction observations and an NWS damage survey are suggestive of both radial outflow and a gust front passage, and model proximity soundings reveal a well-mixed surface layer topped by a strong inversion and large low-level vertical wind shear. Despite the greatest risk of severe winds forecast to be northeast of Colorado, convection-allowing model forecasts from 6 to 18 h in advance did show similar structures to what occurred, warranting further simulations to investigate the unique mesoscale and misoscale features associated with the macroburst.

SIGNIFICANCE STATEMENT: A macroburst occurred in the early morning hours of 9 June in Akron, Colorado, causing extensive damage and widespread power outages. The macroburst and related wavelike features were captured at high resolution by several weather observation stations in the surrounding area and reveal unprecedented oscillations in both temperature and pressure on scales of seconds. The strongest convective wind gusts in Colorado history were also recorded at a 10-m tower outside of Akron, in excess of 50 m s⁻¹. Atmospheric soundings show low-level moisture and dry air aloft, but a sharp low-level temperature inversion that is not typical of a downburst profile. Observational and modeling analyses reveal the potential for gravity wave interactions in addition to strong radial outflow from the macroburst and motivate further work to investigate the complex small-scale processes of this event.

KEYWORDS: Mesoscale processes; Downbursts; Convective storms; Convective-scale processes; Radars/Radar observations; Surface observations

1. Introduction

Just after 0600 UTC [midnight mountain daylight time (MDT)] on 9 June 2020, a macroburst with measured wind gusts of up to 51.12 m s⁻¹ (114.35 mph) impacted the small town of Akron, Colorado, located ~150 km northeast of Denver on Colorado's eastern plains (Fig. 1). Structural and vegetative damage was widespread, but thankfully no injuries were noted among the town's 1700 residents. Very high-frequency data collected from surface weather stations reveal unprecedented near-surface pressure surges and temperature oscillations as the macroburst outflow passed, and the relatively high spatial density of observations makes this event arguably the best observed macroburst in recent memory. The event also created a forecasting challenge, as synoptic and

Supplemental information related to this paper is available at the Journals Online website: https://doi.org/10.1175/MWR-D-20-0412.s1.

Corresponding author: Samuel J. Childs, sam.childs20@alumni. colostate.edu

mesoscale environments did not intuitively prognose a significant wind event for northeastern Colorado, with a deep near-surface stable layer, a cold postfrontal air mass, and the overnight timing. Given the continued reliance—even in recent downburst literature—on measurements from field campaigns conducted in the 1970s and 1980s, the Akron observations have potential to greatly increase understanding of downburst processes and provide a source for verification of high-resolution modeling of such events.

As first defined by Fujita (1978), a downburst is an intense thunderstorm downdraft that produces severe wind gusts and accompanying damage upon reaching the surface with horizontal dimensions not exceeding 10 km. Downbursts are classified as *microbursts* when their horizontal dimensions are less than 4 km and *macrobursts* when greater than 4 km (Fujita 1981, 1985; Hjelmfelt 2010; NSSL 2020). Downbursts¹ are a

¹To avoid confusion, this paper will primarily use the term *downburst* when discussed in a general sense to encompass both microbursts and macrobursts, unless cited literature specifically uses one of the more specific terms.

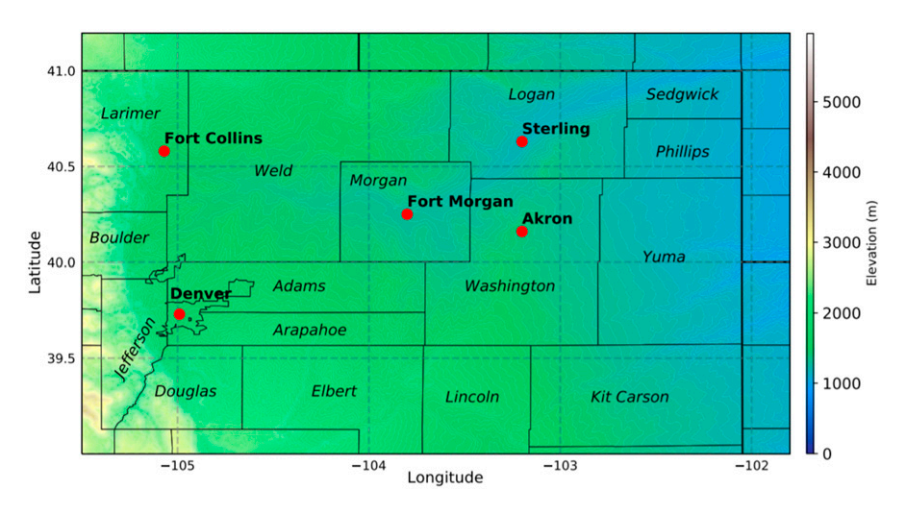


FIG. 1. Topographical depiction of region of interest with county names in italics and select cities and towns in bold.

well-documented aircraft hazard, and their discovery stems from a series of aviation accidents in the mid-twentieth century and specifically the 24 June 1975 Eastern Airlines Flight 727 crash at New York's JFK Airport, which killed 112 people (Fujita 1978, 1990; Hjelmfelt 2010). Damage to vegetation, crops, and physical buildings are also threats from downburst outflows (Hjelmfelt 2010). Downburst damage patterns often resemble those produced by tornadoes (Forbes and Wakimoto 1983), with vegetation flattened in a circular or starburst pattern (Fujita 1990). The Akron event qualifies for a macroburst, thanks to four measured wind gusts in excess of 35.76 m s⁻¹ (80 mph) from four different instruments over a distance of ~5 km.

Fujita's pioneering work inspired several field campaigns in the late 1970s and 1980s that specifically targeted downburst observations and unveiled much of what is known about their physical and environmental features. In 1978, the Northern Illinois Meteorological Research on Downdrafts (NIMROD) project used Doppler radar to detect over fifty downbursts in the Upper Midwest. Wakimoto (1982) used NIMROD data to sketch a life cycle of a gust front produced from a strong downdraft, which begins with a pressure surge and wind direction shift, followed by an uptick in wind speed and falling temperatures within the downdraft region. A dome of high pressure was also found to exist below the main convective downdraft, which is explained in part to hydrostatic cooling as liquid water is evaporated and in part to nonhydrostatic fluid strain as the air decelerates upon approaching the surface (Markowski and Richardson 2010). Thermodynamically, this high pressure dome forces descending air to diverge outward at the surface toward areas of lower pressure, resulting in the aforementioned circular damage pattern.

A second project, the Joint Airport Wind Shear (JAWS) venture, was based out of Denver, Colorado, in the early 1980s (McCarthy et al. 1982). Among other contributions, JAWS led to the distinction between dry and wet microbursts, defined according to the absence or presence of surface precipitation at

the onset of and after the microburst passage.² Wakimoto (1985) and Hjelmfelt (1987) noted that dry microbursts observed during JAWS tended to occur on days that featured a near-surface radiation inversion that decayed during the day, overlain by a dry-adiabatic boundary layer, forming a so-called inverted-V profile on an atmospheric sounding. On the other hand, wet microbursts sampled during the Microburst and Severe Thunderstorm (MIST) project in the Southeast in 1986 were characterized by a moist and stable thermal profile, particularly in lower levels, capped by a dry layer (Atkins and Wakimoto 1991), and radar observations showed that melting hail contributed to negative buoyancy and intense downdrafts (Wakimoto and Bringi 1988). Atkins and Wakimoto (1991) also cited days with high vertical wind shear as more likely to yield microburst-producing storms, compared to days with lower vertical wind shear. More generally, Wakimoto (1985) explored how downbursts rely upon the generation of negative buoyancy, most commonly via latent cooling (i.e., evaporation, melting, or sublimation) and/or hydrometeor loading (Markowski and Richardson 2010; Orf et al. 2012). Seminal work by Rotunno and Klemp (1982) and Klemp (1987) also showed that downward accelerations occur in supercell thunderstorms with strong vertical wind shear because of the orientation of dynamic pressure perturbations: air will generally be forced downward from high pressure perturbations near the middle of the parent storm, concurrent with the most intense updraft speeds.

Around the same time, Fujita (1981) categorized microbursts as either stationary or traveling. He described stationary microbursts as occurring when cold downdraft air accumulates near the surface and displaces the strongest outflow winds above the surface over time. Conversely, his traveling downburst leaves the region of cold air and high pressure behind, allowing the strongest winds to fully descend to the surface and race outward ahead of the cold air dome.

² Technical definitions of *wet* and *dry* microbursts vary somewhat among the literature. For a good discussion, see Wakimoto (1985).

From a modeling perspective, Proctor (1988) used conditions from a JAWS case from 30 June 1982 to produce novel simulations of a macroburst. He found that cooling due to evaporation of rain and melting of hail drove strong downdrafts and a precipitation shaft toward the surface, and cool air at the surface allowed for intensification of the generated ring vortex, which spread out in a circular pattern upon reaching the surface. A nose of high pressure appeared below the downdraft, which raced radially outward ahead of the strongest outflow winds. Proctor's simulations also revealed a relationship between outflow speed and near-surface temperature, namely that as the temperature departure from ambient increased (i.e., became cooler), peak outflow speed increased. A secondary peak in wind speed was also noted within the macroburst outflow next to the precipitation shaft as the initial outflow expanded radially outward. More recently, real-time simulations at high resolution using the Weather and Research Forecasting (WRF) Model (van Dijke et al. 2011; Bolgiani et al. 2020) and idealized simulations (Vermeire et al. 2011; Orf et al. 2012; Oreskovic et al. 2018) have attempted to determine the microphysical and thermodynamical schemes that best match downburst observations. Biernat and Orf (2014) specifically explored wet microbursts by simulating environments with and without a dry layer aloft and found stronger downdraft velocities and surface outflow speeds without the dry layer. Moreover, hydrometeor drag resulting from heavy precipitation played a larger role than evaporative cooling in producing strong downdrafts.

Since the concentrated efforts in the 1970s and 1980s to forecast and diagnose downburst events within funded field campaigns, relatively little observational or diagnostic research has been performed on real cases. Thus, the numerical modeling of downbursts still relies for the most part on the seminal field campaigns for observations and environmental characteristics (Proctor 1988; Lin et al. 2007; Vermeire et al. 2011; Bolgiani et al. 2020). Moreover, existing aviation detection systems continue to be based on what was learned in these early projects (Gultepe et al. 2019). High-resolution observations of destructive downbursts in the United States are lacking in recent literature, although downbursts in Finland (Järvi et al. 2007) and Italy (Burlando et al. 2017) were captured at 10-Hz resolution, albeit with wind speeds of much lesser intensity than the Akron case. The Akron macroburst event therefore has potential to bridge this high-resolution observational gap with arguably the most comprehensive observational analysis of a macroburst in recent decades, thanks to ultra-highresolution near-surface data.

2. Colorado severe convective wind climatology

The magnitude of the Akron macroburst winds can be compared to the national and local convective wind archives compiled in *Storm Data* and maintained by the Storm Prediction Center (SPC; available online at http://www.spc.noaa.gov/wcm). The SPC defines a "severe" wind gust as \geq 50 kt (26 m s⁻¹, 58 mph) and a "significant" wind gust as \geq 65 kt (33.4 m s⁻¹, 75 mph). Reports of thunderstorm wind damage often include downed power lines or trees, structural damage, flattened

crops, or overturned vehicles. The convective wind database currently contains both estimated and measured gusts for the period 1955–2018. Edwards et al. (2018) pointed out that multiple reporting biases exist, including the propensity for gust values to end in "0" or "5" and nonmeteorological geographical hot spots of high winds. Moreover, discontinuities exist across NWS office boundaries (Doswell et al. 2005). Despite these limitations, *Storm Data* offers the most reliable compilation of severe convective wind gusts and damage reports.

In the recent period of 2000–18, when severe convective wind data are considered more reliable (Edwards et al. 2018), Colorado averaged 95 severe convective wind reports each year. This is considerably more than the state's annual average tornado reports (37), but much less than its annual average severe hail reports (267) over the same time period. Colorado has eight convective wind gusts of at least $100 \,\mathrm{kt}$ (51.4 m s⁻¹, 115 mph) in the database, the highest of which was erroneously reported as a wind gust rather than a hailstone diameter and has been flagged for removal. With this report excluded, the highest wind gust is 105 kt (54 m s⁻¹, 120.8 mph) from 28 May 2001 in El Paso County. The next six highest wind gusts are 100 kt, and none of these top seven reports were documented as being explicitly measured. The highest measured gust in the Colorado archives until the Akron event was $96 \,\mathrm{kt} \, (49.4 \,\mathrm{m \, s}^{-1},$ 110.5 mph), but measured wind gusts of 50.45 and $45.6 \,\mathrm{m\,s^{-1}}$ during this event have thus become the first and third strongest convective wind gusts in state history, per the Storm Data archive.³ These two gusts also rank in the 99th percentile for U.S. severe convective wind gusts over the period 2000-18, with the $50.45 \,\mathrm{m\,s^{-1}}$ gust the 12th strongest.

It is also uncommon to have multiple significant severe wind gusts measured at different stations on the same day from the same storm in Colorado, but five separate weather stations in Akron measured wind gusts in excess of 35 m s⁻¹ (79 mph) over the course of approximately 3 min. Interestingly, 3 days earlier a derecho tracked across the entire state, producing a new daily state record of 17 significant severe wind gust reports (Schumacher 2020). Each of these gusts was less than those from Akron, aside from a 49.2 m s⁻¹ (110 mph) high-altitude gust in Winter Park which originated under a very different environmental setup.

3. Event overview

a. Synoptic and mesoscale environments

The national perspective at 0000 UTC (Fig. 2) shows an upper-level trough with its axis near the Four Corners region and strong southwesterly flow approaching $50 \, \text{kt} \, (25.7 \, \text{m s}^{-1})$ ahead of the trough. A broad ridge is situated over the eastern

 $^{^3}$ As of this writing, the 50.45 m s $^{-1}$ gust has been accepted by the SPC for admission into *Storm Data*. The 51.12 m s $^{-1}$ gust from the EC tower was not submitted to SPC since it was measured from 2.3 m AGL and is an instantaneous measurement rather than the traditional 3-s temporal average.

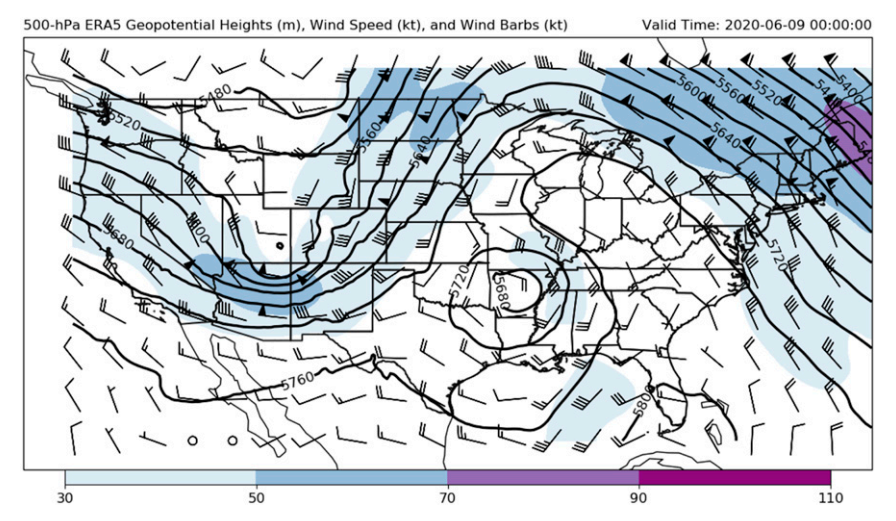


FIG. 2. 500-hPa heights (m), wind speed (kt), and wind barbs (kt) valid at 0600 UTC 9 Jun 2020, from the ERA5 reanalysis. A full line on the wind barb represents 10 kt, and a black flag represents 50 kt.

half of the country, and the low pressure center located over Arkansas is associated with Tropical Depression Cristobal, which was tracking northeastward at this time after making landfall a day earlier.

At the surface, the evening of 8 June 2020 across eastern Colorado featured dropping temperatures in a postfrontal air mass. By 0000 UTC, showers developed across northern Colorado in the statically stable low-level environment, while strong convection was occurring across Nebraska (Fig. 3a). Heavy snow had also begun in the Rocky Mountains at this time, which accumulated up to 15 inches in some locations. A second, primary cold front is depicted directly behind the initial front at 0300 UTC (Fig. 3b), which brought in a cold air mass and resulted in an impressive temperature gradient, from 31°C in southeastern Colorado to 7°C near the Wyoming border. Very strong low-level northerly winds (in excess of 40 kt; 1 kt $\approx 0.51 \,\mathrm{m\,s^{-1}}$) are also evident behind the primary cold front in northern Colorado, along with a strong sea level pressure gradient near the foothills. In fact, between 0300 and 0600 UTC, pressure rose by ~12 hPa at many northern Colorado stations.

A strong thunderstorm formed in the postfrontal environment in central Weld County by 0240 UTC, prompting the evening's first severe thunderstorm warning (SVR). This storm had moved into the Nebraska panhandle by 0300 UTC (Fig. 3b), but several other north-south-oriented streaks of convection were initiating at this time, stretching from the foothills east into Nebraska. By 0500 UTC, the convection of interest formed in western Lincoln County, Colorado, with individual cells moving due north. The northernmost cell in this streak intensified as it entered Washington County from the south, prompting a SVR for Washington and Morgan Counties at 0555 UTC. The SVR polygon was placed west of the town of Akron, but in the following minutes the storm suddenly expanded eastward and took on a bowing structure, accelerating toward the northeast and producing extreme

macroburst winds in the Akron area by 0610 UTC (Fig. 3c). The storm of interest was warned again at 0645 UTC as it moved into Logan County (Fig. 3d), and after producing scattered wind damage southeast of Sterling, it eventually collapsed around 0800 UTC in southeast Wyoming.

Focusing on the time of the macroburst occurrence near Akron from the KFTG radar some 120 km southwest of Akron (Fig. 4), the storm of interest that was displaced west of Akron at 0602 UTC (Fig. 4a) extended eastward by 0612 UTC and acquired a tight bowing signature directly over Akron (roughly between the "A" and the "U" annotations in Fig. 4), which is apparent at 0617 UTC (Fig. 4e). Radial velocity at approximately the equivalent times reveals a rapid shift in wind direction that develops at the leading edge of the bowing segment, most apparent at 0612 and 0617 UTC (Figs. 4d,f), at an elevation of \sim 2 km AGL. This broadly corresponds to the rapid shifts from northerly to west-southwesterly and then back to northerly with the downburst, discussed in more detail below. This sharp divergence implies convergence aloft, above the inversion, and is consistent with downdraft production. Both inbound and outbound radial velocities are observed in excess of $35 \,\mathrm{m \, s^{-1}}$ at this level as the storm passed over Akron. Animations of both reflectivity and radial velocity from KFTG between approximately 0500 and 0730 UTC are available as supplemental material.

The storm that produced the macroburst was one of several on this night displaying wavelike structures. At least nine separate narrow "fingers" of convection can be seen along a southeast-to-northwest corridor from northeastern Colorado into central Nebraska by 0600 UTC (Fig. 3c). Such a pattern is evidence for the possible existence of ducted gravity waves supported by a highly stable layer in the atmosphere. Markowski and Richardson (2010) describe how these waves can serve as a trigger for new convection and thereby produce an alternating pattern of convective fingers and clear air. Gravity waves have also been associated with the evolution

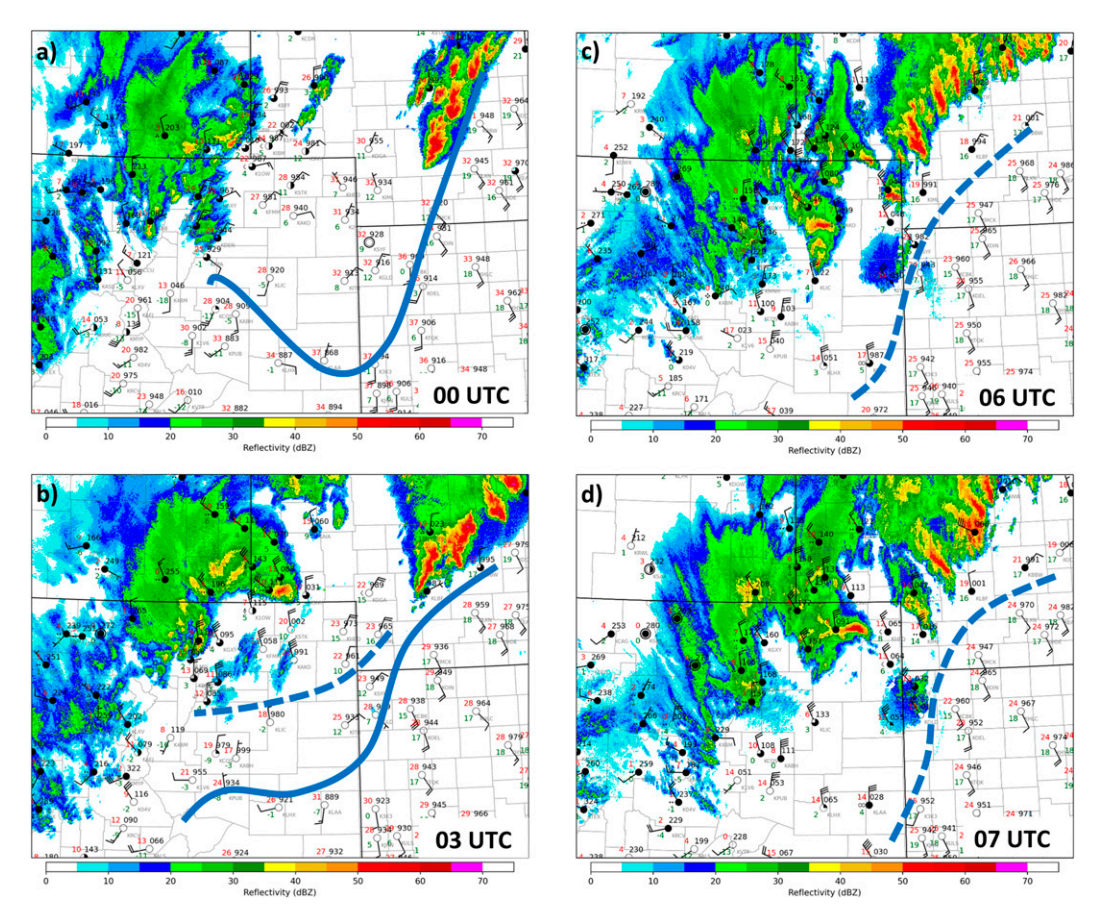


FIG. 3. Surface observations and composite radar reflectivity (dBZ) from the Multi-Radar/Multi-Sensor project for (a) 0000, (b) 0300, (c) 0600, and (d) 0700 UTC 9 Jun 2020. The main cold front and secondary cold front are depicted in dashed and solid blue lines, respectively.

and maintenance of mesoscale convective systems and bow echoes (Metz and Bosart 2010; Adams-Selin and Johnson 2013; Adams-Selin 2020a, 2020b) and initiation of new convection when produced by prior storms (Marsham et al. 2011; Chasteen et al. 2019). Interestingly, each convective finger across Nebraska remained oriented with a north-south component, whereas the Akron storm began similarly but then evolved into an east-west orientation, nearly perpendicular to the overall storm motion. The question becomes what caused this storm in particular to suddenly elongate in the longitudinal direction, contrary to every other convective feature in the larger pattern.

b. Atmospheric soundings

Radiosonde data reveal that favorable ingredients for strong thunderstorms and even downbursts were in place. Although the Akron macroburst occurred between sounding launch times, the North Platte (LBF) sounding from 1200 UTC the following morning was representative of a wet microburst (Fig. 5; Atkins and Wakimoto 1991) despite it being after the main round of convection. In fact, two convective "fingers" are still seen on the LBF radar reflectivity from the same time (not shown); therefore, the environment may not have been completely modified by the convection and cold front, resulting in a

profile that shows characteristics of a wet microburst. The layer from the surface to 675 hPa is very stable, with temperatures holding between 5° and 10°C, above which is a deep dry layer. Very strong 0–6-km wind shear is present (84.3 kt), with a very sharp shift in wind direction from northerlies to southerlies just below the dry layer around 750 mb. Only the most unstable (MU) parcel has any appreciable CAPE (397.5 J kg⁻¹).

Proximity soundings are also generated using the Rapid Refresh (RAP) model for the grid point nearest Akron (~6 km southeast of KAKO). Figure 6 shows a progression of analysis soundings (i.e., forecast-hour zero) and hodographs for 0000, 0500, and 0600 UTC at this grid point. Six hours before the macroburst event (Fig. 6a), warm and dry conditions are noted at the surface, which gradually cool with height but lack moisture throughout the profile. Weak easterly surface winds in advance of the cold front gradually veer and strengthen to southerlies aloft. At 0500 UTC (Fig. 6b), when convection has initiated south of Akron, there is now significant surface cooling overlain by a relatively moist layer between 800 and 700 mb, as well as strong vertical wind shear, with surface northwesterlies veering to southerlies aloft. Again, the change in wind direction is sharpest near the lower boundary of the dry layer aloft. The SPC mesoanalysis for this event (archived at

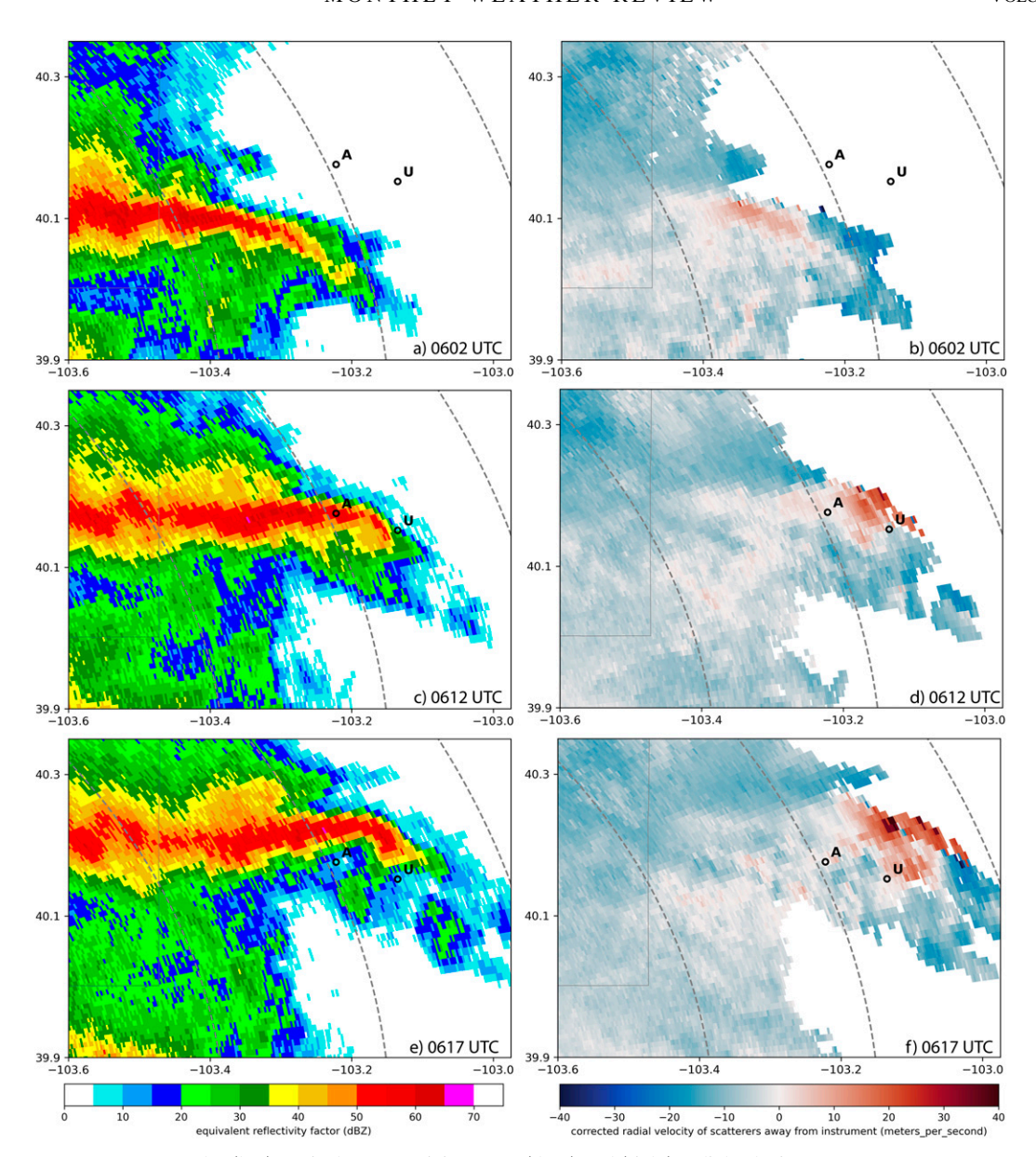


FIG. 4. KFTG radar (left) equivalent reflectivity factor (dBZ) and (right) radial velocity of scatterers away from the radar (m s $^{-1}$). Three sequential times are shown that match within a few seconds between reflectivity and radial velocity: (a),(b) 0602; (c),(d) 0612; and (e),(f) 0617 UTC. The two open black circles represent the locations of KAKO (A) and USDA towers (U). The elevation angle shown is 0.5°, and range rings are shown at 100, 120, and 140 km. The velocities in (b), (d), and (f) were dealiased using the region-based method from the PyART package (Helmus and Collis 2016).

https://www.spc.noaa.gov/exper/archive/event.php?date=20200608), which uses a surface objective analysis scheme merged with RAP upper-air forecast and analysis data on an hourly basis, also reveals a narrow corridor of 0–6-km shear up to 90 kt across eastern Colorado at this time (not shown). The 0600 UTC sounding (Fig. 6c), indicative of the approximate environment when the macroburst occurred, is similar to that of 0500 UTC except for additional surface cooling, which culminates in a shallow mixed boundary layer overlain by a layer of nearly saturated and stable conditions between ~800 and

700 mb (1 mb = 1 hPa), with a temperature inversion in this layer. Elevated instability exists above \sim 675 mb, with the 0500 and 0600 UTC soundings generating 471 and 407 J kg⁻¹ of MUCAPE, respectively. It is interesting to note the absence of a sharp drop in dewpoint in the "dry layer" aloft in these soundings, which Biernat and Orf (2014) found to produce stronger downburst winds relative to a more well-defined dry layer. The very strong directional (and, to a lesser degree, speed) shear and the low-level near-saturated layer also fit typical wet microburst sounding characteristics. Unlike the

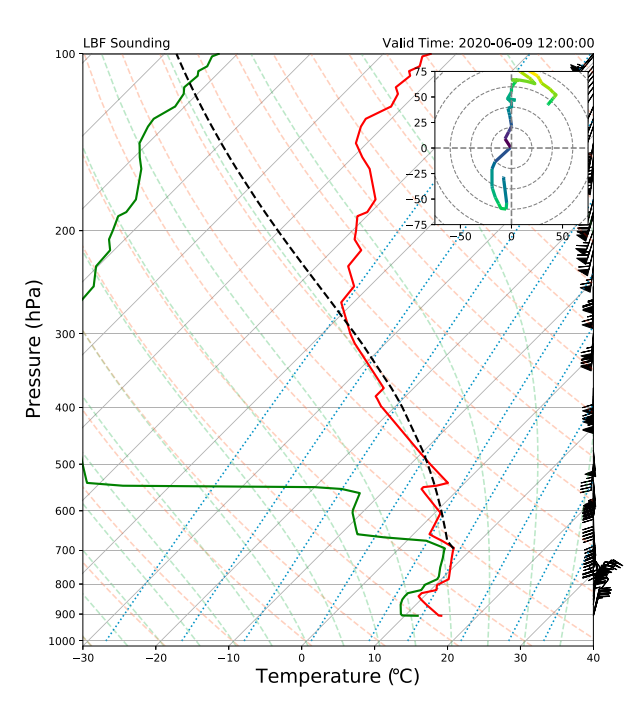


FIG. 5. North Platte (LBF) sounding for 1200 UTC 9 Jun 2020. The solid dashed line represents the most unstable parcel. Wind barbs are in knots, where a flag represents 50 kt, a full barb is 10 kt, and a half barb is 5 kt.

Atkins and Wakimoto (1991) microburst environments, however, the RAP soundings show a high static stability at low levels, with isothermal or increasing temperatures with height at 0500 and 0600 UTC between 800 and 700 mb.

The Scorer parameter l (m⁻¹) is defined formally as

$$l^{2}(z) = \frac{N^{2}}{(U-c)^{2}} - \frac{\partial^{2} U}{\partial z^{2}} / (U-c), \qquad (1)$$

where the first term is a measure of atmospheric stability and the second term a wind curvature term. The term N is the Brünt–Vaisala frequency, U is the wind profile projected onto the plane of motion (from southwest to northeast), and c is the gravity wave speed (estimated as $13.3\,\mathrm{m\,s^{-1}}$ from observations). Equation (1) can be used to assess the potential for ducted gravity waves, or those which are trapped between two stable layers. A Scorer parameter that decreases rapidly with height, typically from reduced stability, is favorable for trapped waves. The Scorer parameter at 0600 UTC is plotted alongside the RAP analysis for this time (Fig. 6c) and shows a spike in magnitude near 750 hPa, corresponding to the temperature inversion. The sharp decline in Scorer parameter above 750 hPa is thus a favorable location for trapped waves, which is an important observation in light of forthcoming analysis.

Another parameter that is sometimes assessed to measure downdraft potential and strength is downdraft CAPE (DCAPE). DCAPE can be calculated by finding the minimum equivalent potential temperature in the lowest 400 hPa and following a parcel down a moist adiabat to the surface from

that value, and Gilmore and Wicker (1998) noted that DCAPE in excess of $1000\,\mathrm{J\,kg^{-1}}$ was associated with strong downdrafts and outflow winds. It should be noted that the DCAPE calculation assumes a parcel descent via latent cooling, but forthcoming modeling analysis will investigate both dynamic and thermodynamic influences (including dynamically driven pressure perturbations as well as latent cooling) on the Akron macroburst environment to see if DCAPE is an appropriate parameter to consider. For example, the SPC mesoanalysis estimated DCAPE $\sim\!800\,\mathrm{J\,kg^{-1}}$ across northeastern Colorado in the predownburst environment, but the RAP analysis soundings reveal that the macroburst occurred in moist and stable low-level conditions. Nevertheless, aspects of both synoptic and mesoscale environments hinted at the potential for downburst production in the convection that formed on this night.

c. Impacts

The SPC convective outlooks on the morning of 8 June outlined their lowest risk of severe weather (MRGL) across the northeastern corner of Colorado, with slight (SLGT) and enhanced (ENH) risks further northeast from central Nebraska through northern Minnesota due to the anticipated high levels of CAPE and bulk shear creating an environment favorable for large hail and strong winds in this area (Fig. 7a). In addition, a 5% severe wind probability contour (not shown) extended into extreme northeastern Colorado, consistent with the larger MRGL risk. While local storm report verification shows that severe weather reports were captured nicely within the convective outlooks northeast of Colorado, the anticipated (and realized) cool postfrontal air mass and low-level stability across northeastern Colorado precluded extension of the SLGT risk into this area. Several wind reports from the Akron event were tallied within the MRGL risk outline (Fig. 7b), but the greatest risk for such destructive winds as were seen was forecast further northeast.

Seventeen reports of either wind damage or a severe wind gust-primarily from two storms-were tabulated across northeastern Colorado on this night, stretching from Akron north and east through Weld, Logan, Yuma, and Phillips Counties. In Akron, an NWS storm survey documented complex damage patterns (National Weather Service 2020). The majority of trees and power lines were felled from southwest to northeast, consistent with outflow or gust front from the larger convective cell which was traveling northeastward. There was also evidence of diverging surface winds in Akron as outflow from the macroburst spread radially outward upon reaching the surface (Forbes and Wakimoto 1983). For example, trees were blown over toward the south at the corner of 1st and Ash Streets, but one block further north, trees toppled toward the north (National Weather Service 2020). At the USDA site east of Akron, trees were blown over toward the east, which would be consistent with both westerly radial outflow and the eastward expansion of the convection itself. Major structural damage was also reported to homes, businesses, vehicles, and farm equipment as well as to aircraft parked at the Colorado Plains Regional Airport, where damage was indicative of southwesterly winds (Fig. 8). Nearby corn and wheat fields

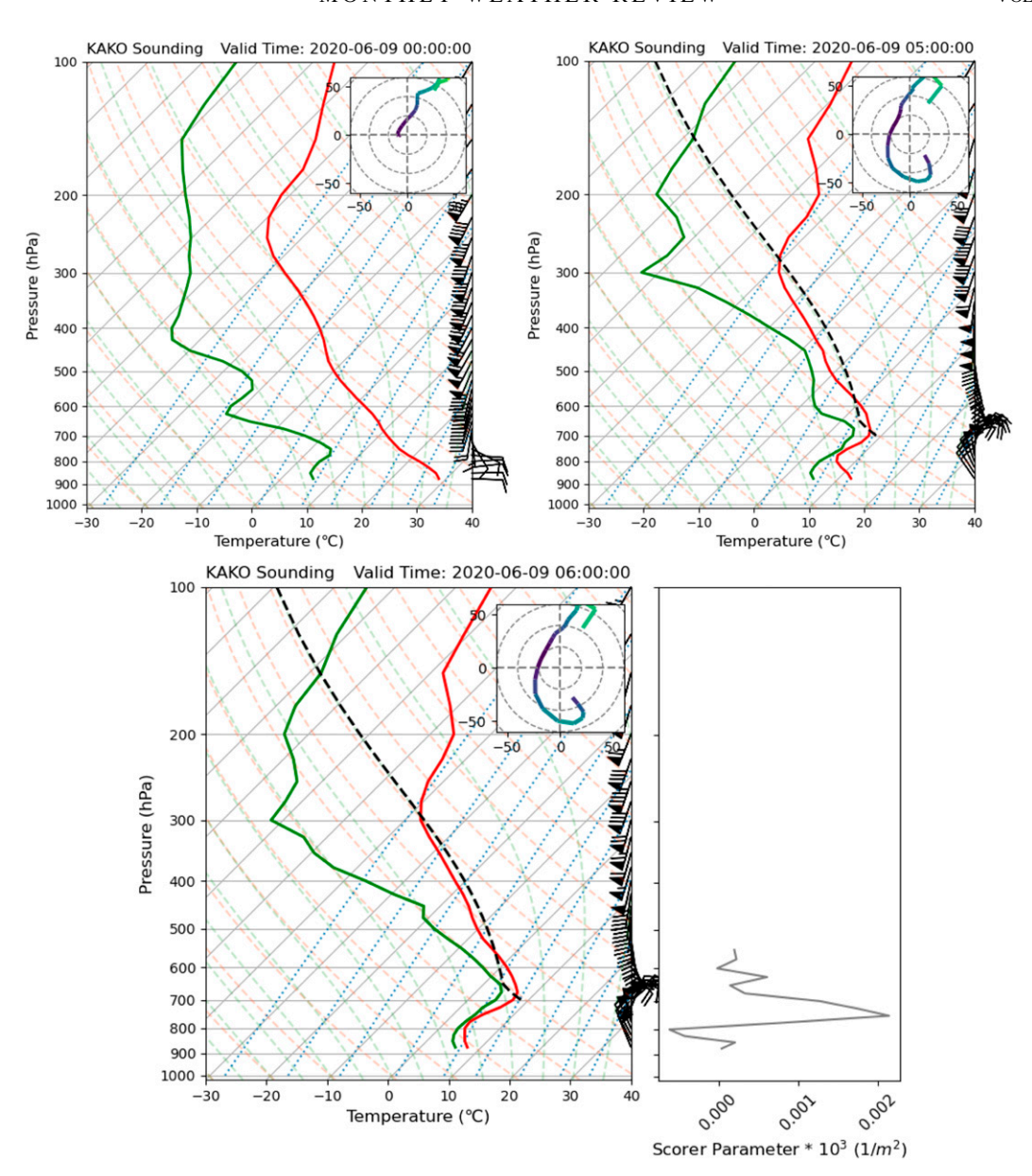


FIG. 6. Proximity soundings generated from the RAP model for analysis times of (a) 0000, (b) 0500, and (c) 0600 UTC 9 Jun 2020 for the grid point closest to Akron. Solid dashed lines in (b) and (c) represent the most unstable parcel. The Scorer parameter is also shown in (c) corresponding to the 0600 UTC sounding and is masked above 550 hPa. Hodographs and wind barbs are in knots, where a flag represents 50 kt, a full barb is 10 kt, and a half barb is 5 kt.

were reportedly stripped by wind-driven small hail (Sedgwick County Office of Emergency Manager 2020), a common occurrence in the landscape of eastern Colorado (Childs et al. 2020). This affirms the presence of an ice-phase component of hydrometeor loading contributing to the downdraft strength.

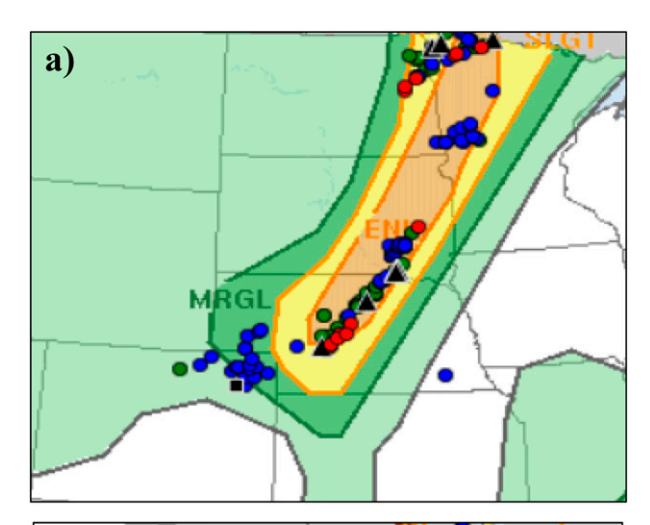
4. Observational analysis

The macroburst happened to occur over an area with several agricultural research facilities that collect meteorological measurements. Figure 9 shows the stations from which data

were used, along with an illustration of the storm's main composite reflectivity core at three sequential times. The high spatial and temporal resolution of the observing stations allows for an in-depth look at the small-scale features of the event that eclipses that of any previous macroburst examination. The names and specifications of the instruments described in the forthcoming paragraphs are given in Table 1 for comparison.

a. Automated surface observing stations (ASOS)

Three ASOS stations near Akron (KAKO), Yuma (K2V6), and Sterling (KSTK) captured elements of the macroburst and



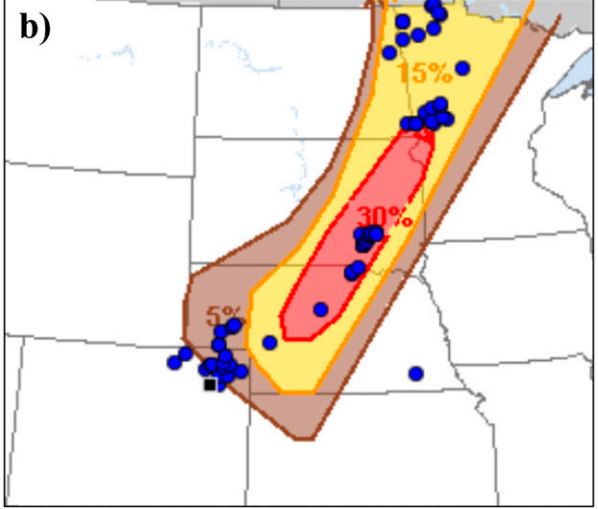


FIG. 7. (a) SPC severe convective outlook and (b) severe wind probabilities issued at 2000 UTC 8 Jun 2020. Local storm report verification is shown for reports between 2000 UTC 8 Jun and 1200 UTC 9 Jun. Blue circles in (b) represent wind reports \geq 50 kt, and black squares represent wind reports \geq 65 kt.

outflow boundary at no finer than 5-min resolution. Of note, each station recorded steadily falling temperatures following the cold front passage in late evening, followed by oscillations in pressure unaccompanied by changes in temperature that could be consistent with gravity waves. While gravity currents (including those brought on by downbursts), gravity waves, and bores are all typically accompanied by an increase in surface pressure (Wakimoto 1985; Proctor 1988; Davis et al. 2004; Adams-Selin and Johnson 2013), gravity current passage is also associated with a corresponding decrease in temperature at a station, whereas gravity waves typically do not induce substantial temperature fluctuations (Haertel et al. 2001).

At KAKO (Fig. 10a), station pressure slowly fell in the evening before leveling off around 845 hPa. The aforementioned cold front passed through KAKO around 0245 UTC, as indicated by the sharp rise in wind speeds and wind direction shift to northwesterly. Station pressure also began to slowly





FIG. 8. (top) Significant damage and power outages reported throughout the town of Akron. (bottom) Damage to an aircraft at Colorado Plains Regional Airport on northern edge of Akron (photos credit: National Weather Service 2020).

rise in advance of the frontal passage. Immediately prior to the station's maximum wind gust $(37.04\,\mathrm{m\,s^{-1}}\ at\ 0610\ UTC)$, pressure spiked by $\sim 7\ hPa$ in only $10\ min$, over which time temperature also rose by $1^\circ\mathrm{C}$. Concurrent with the pressure surge, wind direction shifted from northerly to southwesterly, which can be explained by both strong outflow from the leading edge of the convective cell and radial outflow from the macroburst descending to its south. It should also be noted that thunder (but not rain) was recorded at KAKO at the time of maximum winds, but radar observations do imply heavy precipitation at KAKO after 0610 UTC, the final observation before KAKO stopped recording due to a power outage.

The town of Yuma, situated 40 km east of Akron, was spared the main convective core but did observe similar characteristics (Fig. 10b). A cool air mass was in place at the surface by 0000 UTC, and a pressure surge of nearly 5 hPa occurred over a 20-min timeframe just prior to K2V6's peak wind gust of 27.78 m s⁻¹ at 0644 UTC. Unlike KAKO, a temperature spike of \sim 2°C occurred after the maximum wind gust. This progression would be consistent with mixing of warmer air aloft toward the surface inside the perimeter of the expanding radial

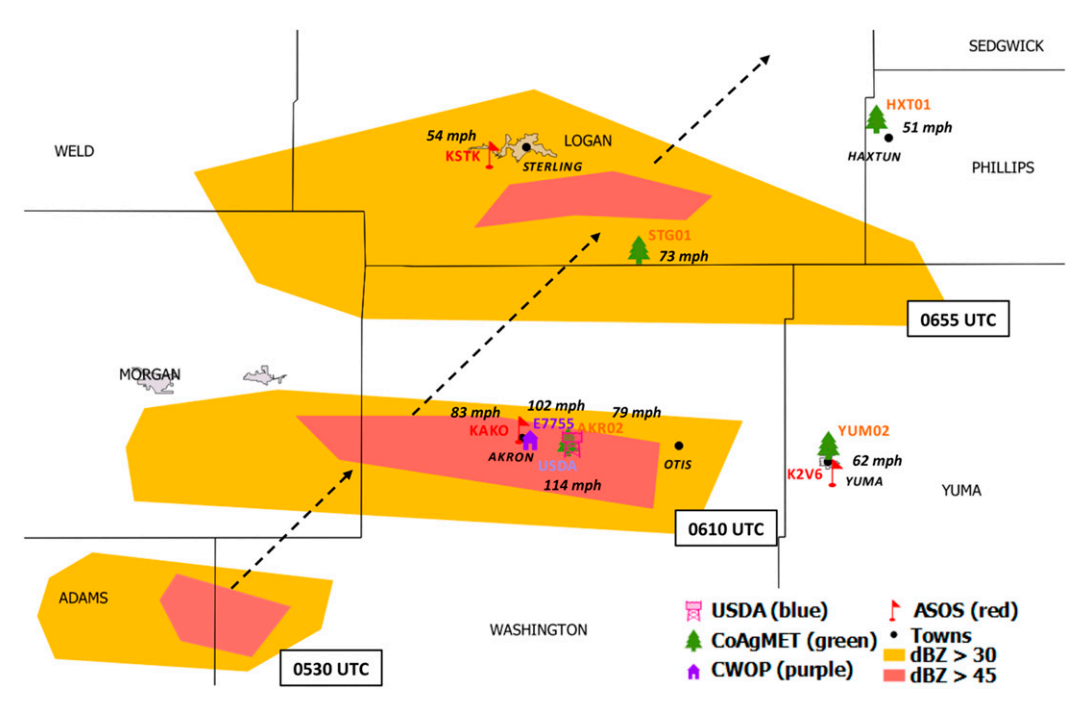


FIG. 9. Illustration of radar reflectivity of macroburst-producing storm. The approximate core of the storm is depicted at three sequential times. Stations referenced in the text are represented according to type. Towns are shown as black dots with italicized labels, county names are in light all-capital letters, and dashed arrows indicate the approximate storm motion. Maximum wind gusts measured at a particular station are also annotated.

outflow from the macroburst. KSTK, located southwest of Sterling, also reported cool air at the surface and a pressure surge of 5 hPa over the 10 min prior to the convective line passage at approximately 0710 UTC (Fig. 10c). However, KSTK's temperature trace was relatively flat, perhaps a result of temperature fluctuations localized to the strongest part of the outflow away from KSTK, or coarser temperature resolution (discussed further in section 6), or both. In addition, the maximum wind gust of the night at KSTK occurred from an earlier severe thunderstorm. It is interesting to note, however, that despite coarser observations, both K2V6 and KSTK recorded a subtle shift in wind direction at the time of the convective outflow, from northwesterly to westerly. The cold frontal passage is also apparent at KSTK, evidenced by the rise in pressure and wind speed at 0230 UTC.

b. CWOP and CoAgMET

Traces of temperature, station pressure, wind speed, and wind gusts from a Citizen Weather Observing Program (CWOP; Creager et al. 2009) home weather station E7755 on the eastern edge of Akron are shown in Fig. 10d at 5-min resolution. It should be noted that the anemometer on this station was situated at 14.5 m AGL, higher than the standard 10-m altitude, and was part of a Davis Vantage Pro weather system, which logs temperature, relative humidity, pressure, and precipitation data at 5-min resolution (station owner, personal communication). Compared to the surrounding stations, the measured winds leading up to the downburst event were up to 10 m s⁻¹ lighter at E7755. While these values at this

home weather station may not be completely reliable, the two consecutive gusts of $45.6 \,\mathrm{m \, s^{-1}}$ (102 mph) and $42.5 \,\mathrm{m \, s^{-1}}$ (95 mph) at 0610 and 0615 UTC, respectively, are arguably even more impressive given the potential low bias in wind speeds leading up to the event. Consistent with the other nearby stations, temperatures fell at E7755 throughout the evening to a minimum of 7.78°C at 0605 UTC, then rose to 8.89°C by 0615 UTC. Station pressure begins to rise with the passage of the cold front, increasing from 844 to 850 hPa over the course of 4 h before decreasing slightly. Then from 0600 to 0610 UTC, immediately prior to the temperature spike and maximum wind gusts, pressure rose from 847.7 to 853.4 hPa. Pressure then plummeted in the next 5 min to 846.0 hPa at 0615 UTC. Wind direction at E7755 remained northerly at each of these observation times, but it is reasonable to believe that the 5-min resolution may mask a quick shift to southerly or westerly winds as the gust front and radial outflow passed. Following the 0615 UTC measurement, the weather station stopped recording due to the power outage.

Four stations—Akron (AKR02), Yuma (YUM02), Sterling (STG01), and Haxtun (HXT01)—are part of the Colorado Agricultural Meteorological Network (CoAgMET; Doesken et al. 1998). These stations record temperature; dewpoint and relative humidity; wind speeds, gusts, and direction; precipitation; and other parameters relevant to the agriculture community, at a temporal resolution of 5 min. Although pressure is not recorded, 5-min temperature and wind gust traces show similar characteristics to other observing stations (Fig. 11). AKR02 has very sporadic observations during this time, due in

TABLE 1. Instrumentation specifications for each category of weather observing station mentioned in the text.

	=		=	
	Error	Resolution	Sampling frequency	Sensor altitude
	USDA EC towe	r—LI-COR LI-7500DS; Gill	3D sonic anemometer	
Pressure	$\pm 0.4\mathrm{kPa}$	0.003 kPa	10 Hz	2.3 m
Temperature	±0.25°C	0.006°C at 25°C	10 Hz	2.3 m
Wind	1.5% at $12\mathrm{ms^{-1}}$	$0.01\mathrm{ms^{-1}}$	10 Hz	2.3 m
	USDA 10-m tower—Campl	pell scientific 107-L; Campbel	l scientific RM young wind sentry	
Temperature	±0.01°C	\sim 0.01 $^{\circ}$ C a	1 min	2 m
Wind	$\pm 0.5\mathrm{ms}^{-1}$	$0.1{\rm ms}^{-1}$	3 s (gust)	10 m
		CWOP—Davis Vantage I	p_{ro}	
Pressure	±1.0 hPa	0.1 hPa	1 min	$\sim 6 \text{ m}^{\text{b}}$
Temperature	±0.3°C	0.1°C	1 min	$\sim 6 \text{ m}^{\text{b}}$
Wind	$\pm 0.45 \mathrm{ms^{-1}}$	5%	3 s (gust)	14.5 m
ASOS			,	
Pressure	±0.67 hPa	0.1 hPa	1 min	2 m
Temperature	±1°C	0.056°C	5-min avg	2 m
Wind	$\pm 0.5\mathrm{ms^{-1}}$	$1 \mathrm{m s^{-1}}$ or 5%	5 s (gust)	10 m
	CoAgMET—Vaisala H	MP45C Probe; Campbell scie	entific RM young wind sentry	
Temperature	±0.2°C	0.1°C	5-min avg	1.5 m
Wind	$\pm 0.5\mathrm{ms}^{-1}$	$0.1{\rm ms}^{-1}$	10 s (gust)	2 m

^a The temperature resolution of the USDA 10-m tower is a function of the datalogger resolution, which is unknown to the authors but estimated to be 0.01°C based on the data output received.

part to the power outage, and is thus not plotted in Fig. 11. Temperature spikes of 1.1°C at STG01 and 1.0°C at HXT01 were measured in the minutes immediately prior to each station's maximum wind gust. Then in the 10 min following their peak gusts, STG01 and HXT01 recorded 3.7° and 2.3°C drops in temperature. While YUM02 shows a more consistent temperature time series, there is a steady rise between 0600 and 0715 UTC and elevated wind gusts during this period. The YUM02 temperature trace is also similar to that of KAKO (Fig. 10a) in its oscillation around the time of the cold frontal passage between 0300 and 0400 UTC.

c. USDA 10-m and EC towers

Finally, two towers located at the USDA Central Great Plains Resources Management site approximately 2 miles east of Akron captured high-resolution temperature, pressure, and wind measurements. A 10-m tower records maximum wind gusts at 10, 5, 2.5, and 1.5 m, as well as temperature at 10, 4, and 2 m, and 10-m wind direction, all at 1-min resolution. The wind gust recorded each minute represents the maximum within a sampling frequency of 5 s. The second tower at the USDA site is an EC flux tower, used to measure vertical gradients in gas concentrations. This tower is fitted with a sonic anemometer at 2.3 m AGL that records instantaneous wind speed at 10-Hz frequency, along with temperature and pressure.

Time series of the 10-m tower data (Fig. 12) reveal that throughout the late evening, wind gusts at each level were consistently around $20\,\mathrm{m\,s^{-1}}$, with slightly higher values at 10-m height compared to 2.5 m. As the downburst winds reached the surface between 0610 and 0613 UTC, wind gusts spiked at each height, to maxima of 50.45 m s⁻¹ at 10 m and 43.7 m s⁻¹ at

2.5 m. In addition, the 10-m wind direction, which had been steady out of the northwest throughout the evening, rotated quickly from northwesterly to southwesterly to northeasterly from 0610 to 0613 UTC. It is also noteworthy that wind gusts continued to be measured at or above severe limits (25.9 m s⁻¹) for a span of nearly 10 min. Temperature traces plotted for 10 and 2 m show steady cooling to a minimum of 7.7°C just before 0600 UTC, followed by an abrupt increase to 10.8°C at 0612 UTC, immediately following the maximum wind gust. Temperatures at each level then fell to a minimum of 6.5°C at both 10 and 2 m over the next 8 min. Two additional temperature spikes occurred around 0624 and 0629 UTC, as temperatures rose to 9°C before slowly decreasing through the rest of the early morning. Each of these temperature spikes was preceded by a subtle decrease in wind speed and wind direction shift; additional analysis is warranted to investigate whether these could be associated with undulations behind the head of a bore or wave breaking (e.g., Rottman and Simpson 1989).

An even finer-scale look at the macroburst passage is made possible with 10-Hz data from the EC tower. Figure 13 shows time series of applicable parameters from 0400 to 0700 UTC, while Fig. 14 zooms in to 0610–0622 to highlight the oscillations. The station pressure trace depicts a rise of 3 hPa over 30 min from 0430 to 0500 UTC (Fig. 13), a signal which is also apparent in the KAKO ASOS time series (Fig. 10a). After leveling off for 1 h, a pressure surge of 6 hPa occurred in 6 min from 0602 to 0608 UTC. A final and most impressive pressure surge occurred immediately after the peak wind gusts, a 5-hPa rise to 864 mb in a mere 19s from 0613:24 to 0613:43 UTC (Fig. 14). In the three subsequent minutes, pressure plummeted to 849 hPa, approximately 5 hPa lower than before the initial

^b The pressure and temperature altitudes at the CWOP station are estimated based on the known anemometer height and typical setup of the Davis Vantage Pro system.

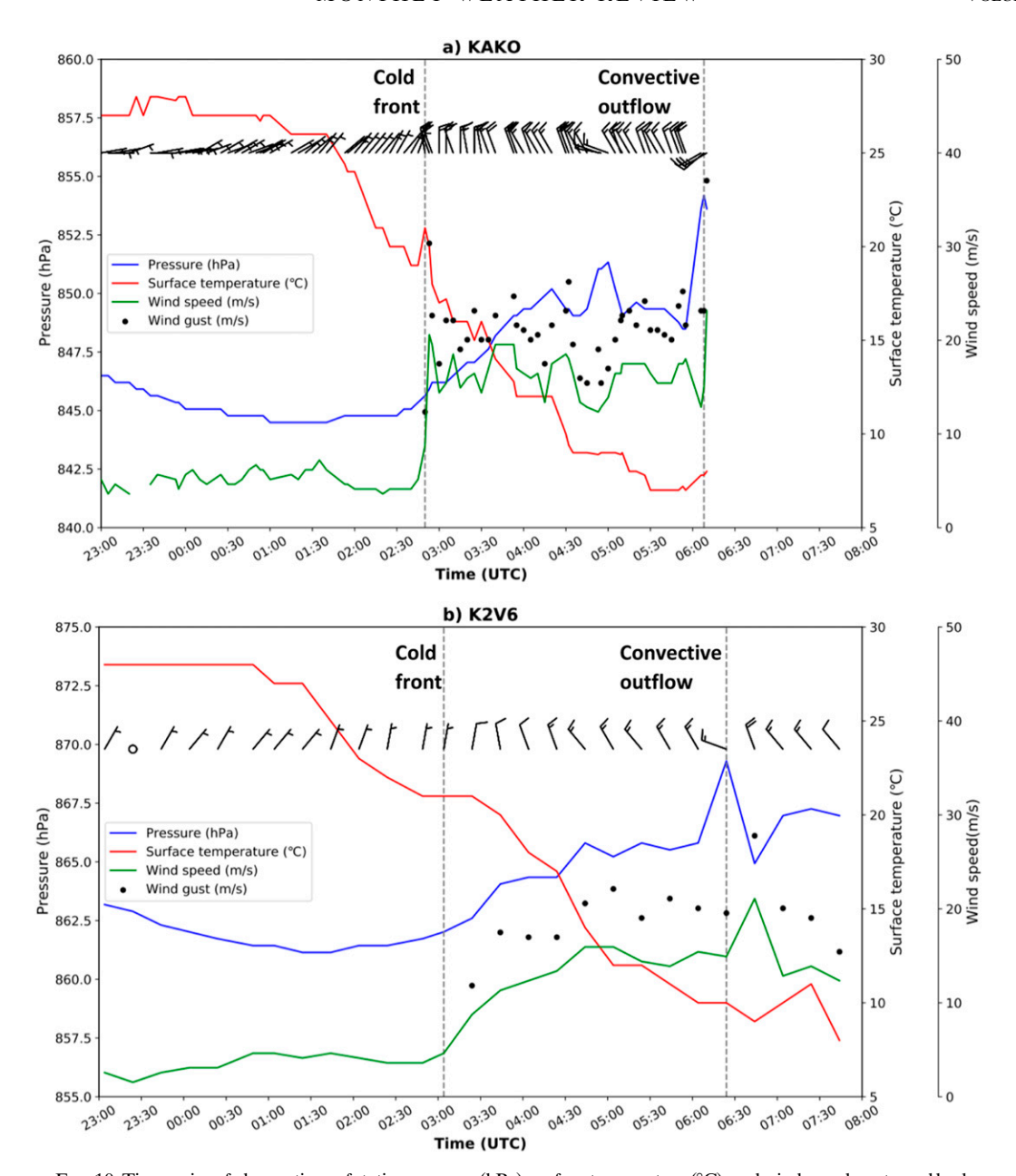


FIG. 10. Time series of observations of station pressure (hPa), surface temperature (°C), and wind speed, gusts, and barbs (m s $^{-1}$) for (a) KAKO, (b) K2V6, (c) KSTK, and (d) E7755 for the night of 8–9 Jun 2020. A full barb represents 10 m s $^{-1}$, and a half barb is 5 m s $^{-1}$. Vertical dashed lines indicate time of secondary cold front passage and convective/macroburst outflow, respectively. Note the range of values for station pressure differs between (a) and (d) and (b) and (c).

pressure surge. After this, pressure rose back to 856 hPa, slightly higher than its level from earlier in the evening. Such extreme pressure undulations exceed previous examples of observed pressure jumps associated with convection in the literature. For example, Coleman et al. (2009) noted a 1.5-hPa pressure surge over 8 min from a bore in Iowa, and Coleman and Knupp (2011) reported a 0.25-hPa pressure jump in 3 min from an undular bore in northern Alabama. Pressure surges on the order of a few hPa have also been observed in advance of the mesohigh and with the rear-flank downdraft of supercell thunderstorms (Johnson

2001 and references therein, Clark et al. 2018). Additional case study analyses have shown pressure surges in the ballpark of 2 hPa in periods less than 30 min with the passage of a bore or other gust front (Koch et al. 1991; Shreffler and Binkowski 1981; Adams-Selin and Johnson 2013; Mueller et al. 2017), but still much smaller than those observed from the 10-Hz data here.

The temperature trace from the EC tower (measured at $2.3\,\mathrm{m}$ AGL) shows a steady decrease in temperature to $7.5^\circ\mathrm{C}$ by $0600\,\mathrm{UTC}$ in the postfrontal air (Fig. 13). However, between $0602\,\mathrm{and}\,0608\,\mathrm{UTC}$ and concurrent with the 6-hPa pressure

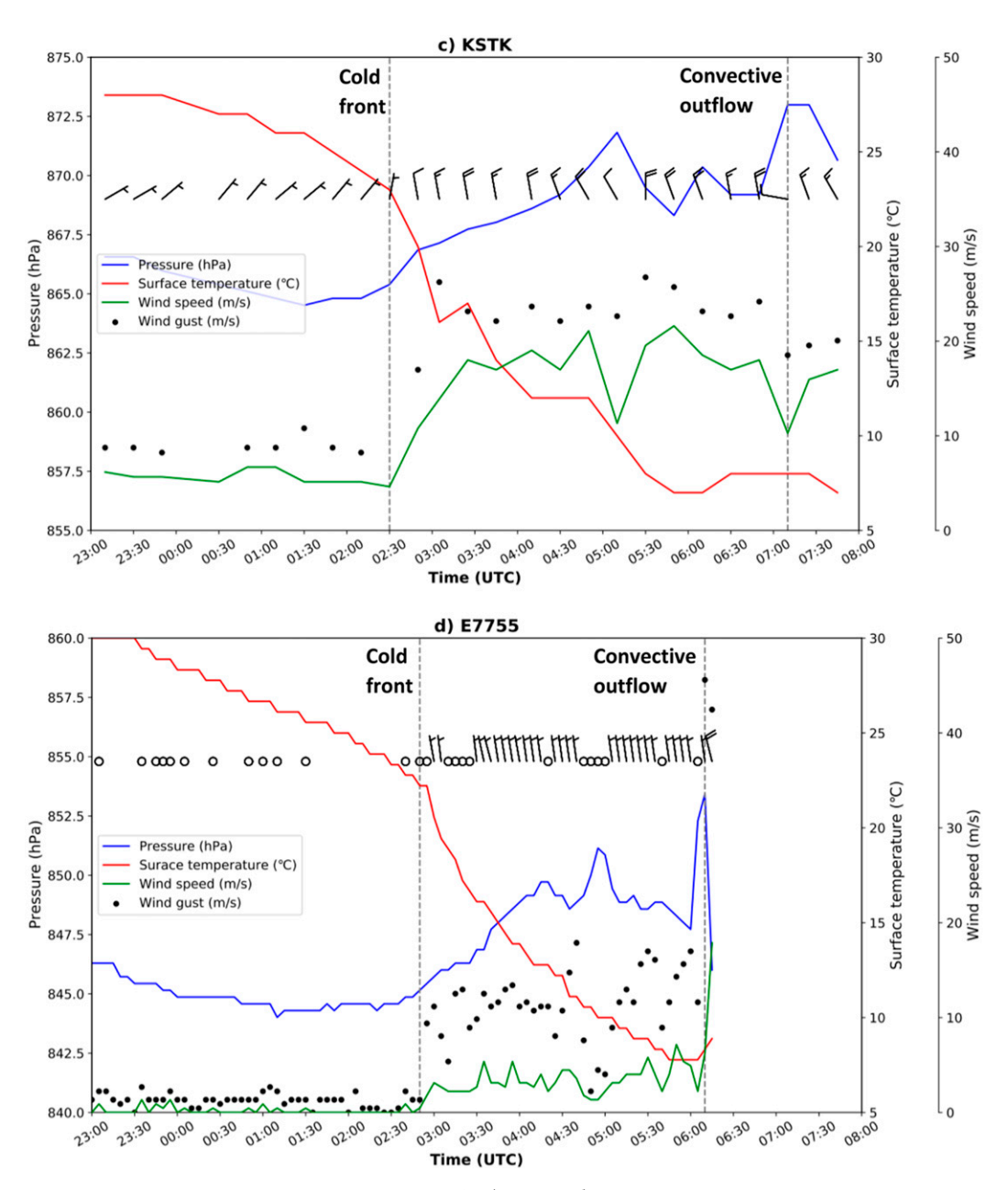


FIG. 10. (Continued)

surge, temperatures rose by approximately 2°C. After a brief cooling, temperature suddenly spiked upward from 8.39° to 10.08°C from 0612:59 to 0613:43 UTC (Fig. 14), concurrent with the 5-hPa pressure surge and maximum wind gusts. Temperature maxed out at 10.23°C at 0616:01 UTC and then quickly fell to a minimum value of 6.4°C by 0617:40 UTC, yielding a 3.83°C oscillation in less than 5 min. A second temperature spike then occurred in the following minute, climbing back to 8.99°C by 0618:40 UTC before finally leveling off.

Instantaneous wind speeds measured by the EC tower at 2.3 m AGL held steady at around $10\,\mathrm{m\,s^{-1}}$ for most of the

evening (Fig. 13). Then at 0612 UTC, wind speeds suddenly escalated as the strong downdraft reached the surface, and a maximum value of 51.12 m s⁻¹ (114.35 mph) was measured at 0613:23.4 UTC (Fig. 14). This timing matches well to the reflectivity depiction shown in Fig. 4, wherein the storm is seen elongating and bowing out at the 0612 UTC scan near KAKO and the USDA site (the "A" and "U" labels in Fig. 4, respectively). Such high-resolution data allow us to pinpoint that temperatures began to rise first, followed by the maximum wind gust and then the 5-hPa pressure surge, all within one minute's time. A second gust of 50.45 m s⁻¹ (112.7 mph) was recorded four seconds after the first at 0613:27.1 UTC as

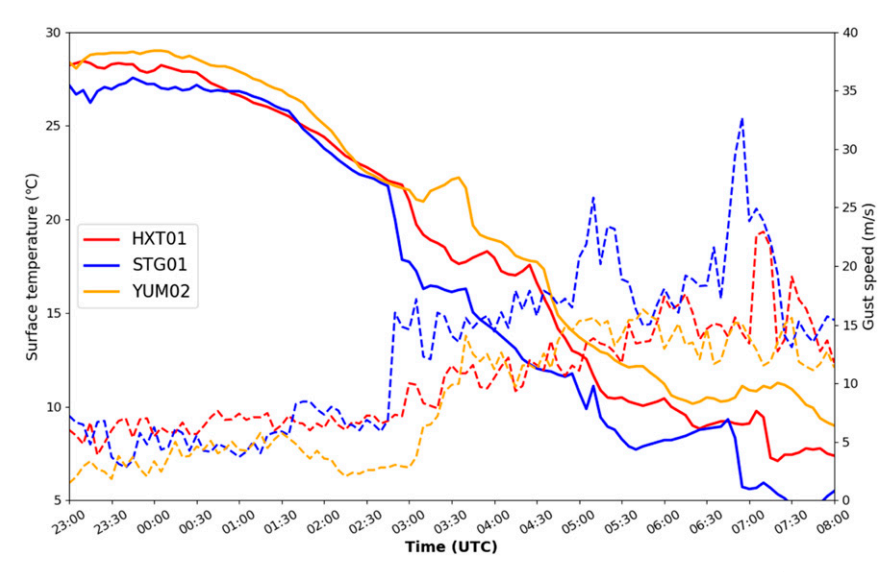


FIG. 11. Time series of surface temperature (lines; °C) and wind gusts (dashes; m s⁻¹) for three CoAgMET stations in the path of the convective outflow.

pressure was spiking upward. As with the 10-m tower, wind direction also rotated from northwesterly to southwesterly to northeasterly over these few minutes. Winds remained elevated at an average of $15~{\rm m\,s^{-1}}$ for 1 h following the peak gusts, after which they calmed to levels comparable to earlier in the evening. Though instantaneous wind speed has been used in fine-scale microburst observations (Järvi et al. 2007), a more conventional 3-s average wind speed was also calculated from the EC tower data, which yielded a maximum gust of $40.86~{\rm m\,s^{-1}}$, comparable to the $43.7~{\rm m\,s^{-1}}$ gust from the nearby 10-m tower at $2.5~{\rm m\,AGL}$. By way of summary,

Table 2 lists the maximum wind gusts for stations that recorded a gust of at least $25 \,\mathrm{m\,s}^{-1}$, as well as the respective frequency and altitude.

The small-scale pressure, temperature, and wind speed fluctuations captured from the USDA towers—and indeed the forthcoming hypotheses regarding their underlying causes—would have been missed by the coarser ASOS-station data and thereby showcase the value of collecting weather data at finer resolutions. In fact, the combination of the 10-Hz and 1-min data are to our knowledge the finest in temporal resolution of any previously analyzed downburst event and thus

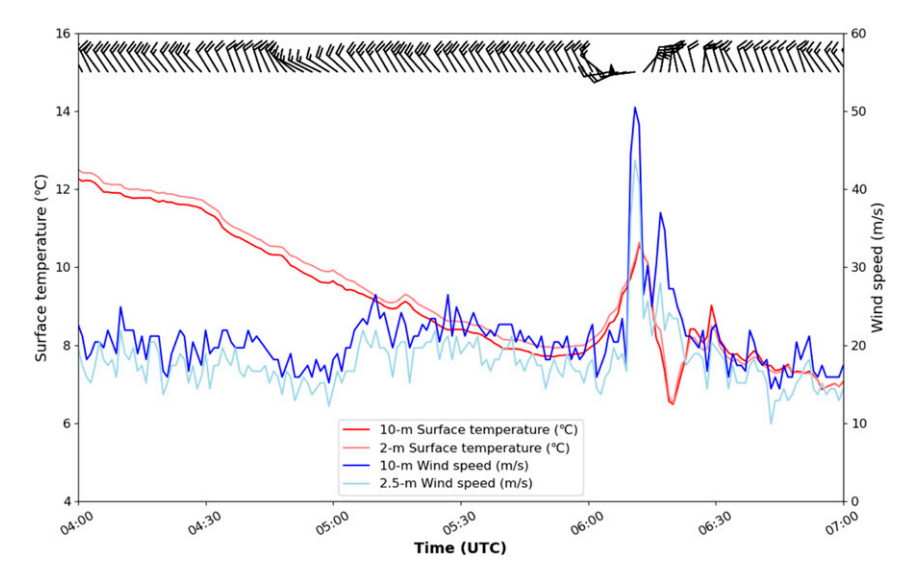


FIG. 12. Time series of surface temperature at 10 and 2 m (°C), and wind speed at 10 and 2.5 m (m s⁻¹) for the 10-m USDA tower. Data frequency is every minute, and wind speed represents the maximum gust from a sampling frequency of 5 s. Wind barb flags represent 50 m s⁻¹, full barbs represent 10 m s⁻¹, and half barbs represent 5 m s⁻¹.

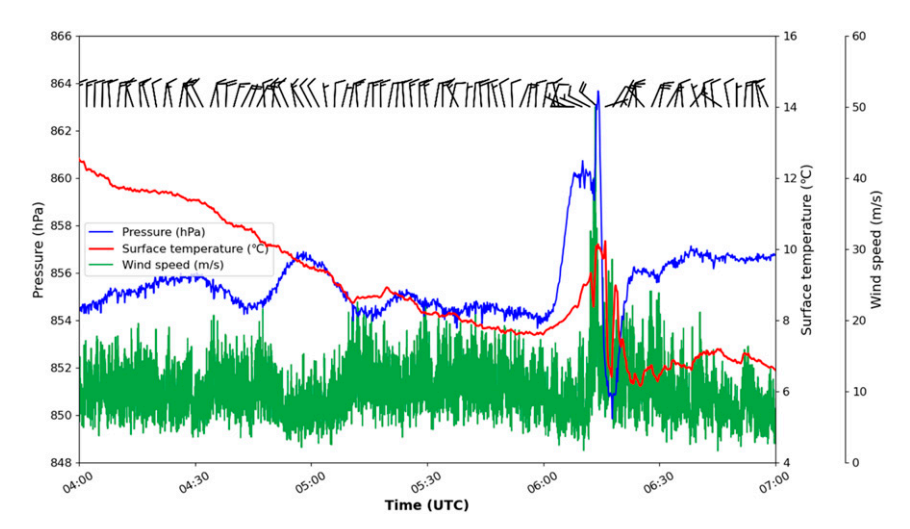


FIG. 13. Time series of surface temperature at 2.3 m AGL (°C), station pressure (hPa), and instantaneous wind speed (m s⁻¹) for the USDA EC tower. All data are at 10-Hz frequency, but for clarity temperature is plotted at 10 Hz, pressure is plotted every second, and wind speed is plotted every tenth of a second. Wind barbs (m s⁻¹) are plotted every 2 min and are of the same convention as those in Fig. 12.

have great worth in understanding the misoscale processes of such high-impact wind events.

5. Convection-permitting model forecasts

Given the complex small-scale processes and oscillations revealed from the observational data, it is of worth to evaluate the performance of convection-allowing models in an event such as this. The High-Resolution Ensemble Forecast (HREF) version 2 (Roberts et al. 2019) creates ensemble output of applicable severe weather parameters from a suite of models at 3-km grid spacing. Two of the ensemble members, namely the

High-Resolution Rapid Refresh (HRRR; Benjamin et al. 2016) and North American Model CONUS Nest (NAM Nest) are highlighted in Fig. 15. The composite reflectivity forecast and updraft helicity swaths > 75 m² s⁻² from the 8 June 1200 UTC run of the HRRR, valid at 0600 UTC 9 June (Fig. 15a), shows several convective "fingers" across Nebraska, with embedded stronger supercells. The 0000 UTC 6-h HRRR forecast (Fig. 15b) extends convection into eastern Colorado, approximately one county east of what verified, and is again indicative of wavelike structures. The NAM Nest simulations of composite reflectivity and associated UH swaths valid at 0600 UTC 9 June (Figs. 15c,d) are similar to observations but

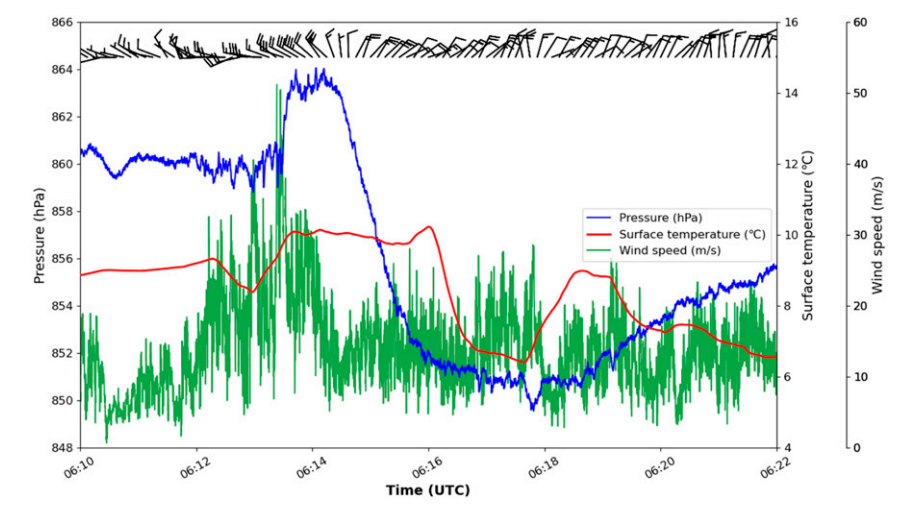


FIG. 14. As in Fig. 13, but for a shorter period of interest. All parameters are plotted at 10-Hz frequency, and wind barbs are plotted every 7.5 s. The $50 \,\mathrm{m\,s^{-1}}$ barb does not show up due to the coarser sampling frequency for clarity.

TABLE 2. Maximum wind gust for each observing station that measured a gust of at least 25 m s ⁻¹ , as well as the frequency of
observations and height of anemometer above ground level.

Station name	Station type	Max wind gust (m s ⁻¹)	Frequency (s)	Anemometer height (m)
USDA EC tower	USDA	51.12	Instantaneous	2.3
USDA 10-m tower	USDA	50.45	3	10
E7755	CWOP	45.6	3	14.5
USDA EC tower	USDA	40.86	3	2.3
KAKO	ASOS	37.04	3	10
AKR02	CoAgMET	35.32	10	2
STG01	CoAgMET	32.63	10	2
K2V6	ASOS	27.78	3	10

with displacement errors, including a storm one county east of Akron that appears to be bowing out with an east-west orientation as opposed to north-south oriented storms further northeast. The HREF also predicts a 10% neighborhood maximum ensemble probability (radius = 40 km) of wind speeds in excess of 50 kt (Fig. 16) valid at 0600 UTC 9 June from both the 1200 UTC 8 June and 0000 UTC 9 June runs across parts of northwestern Colorado, although the highest probabilities are north and west of Akron and the ensemble maximum wind speeds (Fig. 16, shading) do not exceed 60 kt in either run. Nevertheless, the fact that the convective wavelike structure was prognosed ~18 h in advance and refined to northeastern Colorado with a strong

bowing segment 6 h in advance of the Akron macroburst event is noteworthy.

In addition to the HREF, the Colorado State University Precipitation Systems Research Group's 4-km real-time Weather and Research Forecasting (WRF) Model forecast (configuration described in Schumacher 2015), initialized at 0000 UTC 9 June, shows a reflectivity depiction of the event similar to observations (Fig. 17), albeit with timing and location errors. At 0600 UTC (Fig. 17a), a large area of convection is simulated east of Akron, with some wavelike structures further northeast in Nebraska. At 0700 UTC (Fig. 17b), the several latitudinal convective fingers are clearly defined across Nebraska, and by 0800 UTC (Fig. 17c), two longitudinal storms

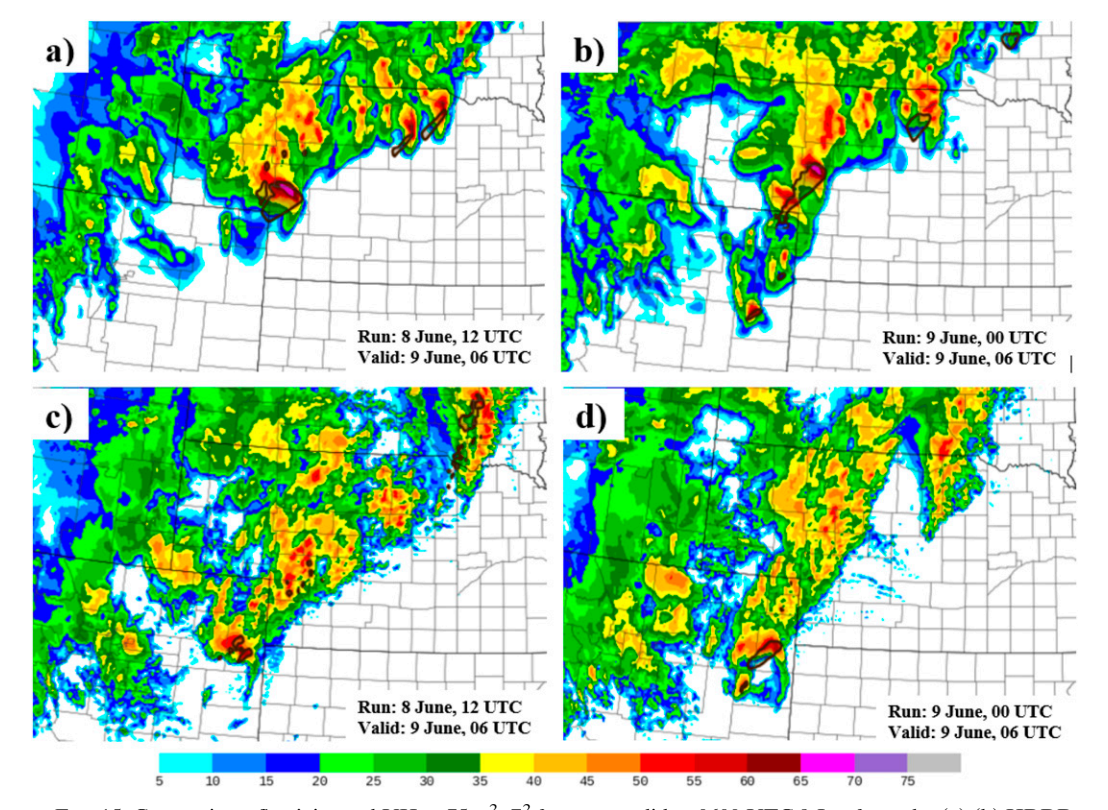


FIG. 15. Composite reflectivity and UH > 75 m² s⁻² forecasts valid at 0600 UTC 9 Jun from the (a),(b) HRRR and (c),(d) NAM Nest models as part of the HREF ensemble. (left) The 1200 UTC 8 Jun forecast and (right) the 0000 UTC 9 Jun forecast.

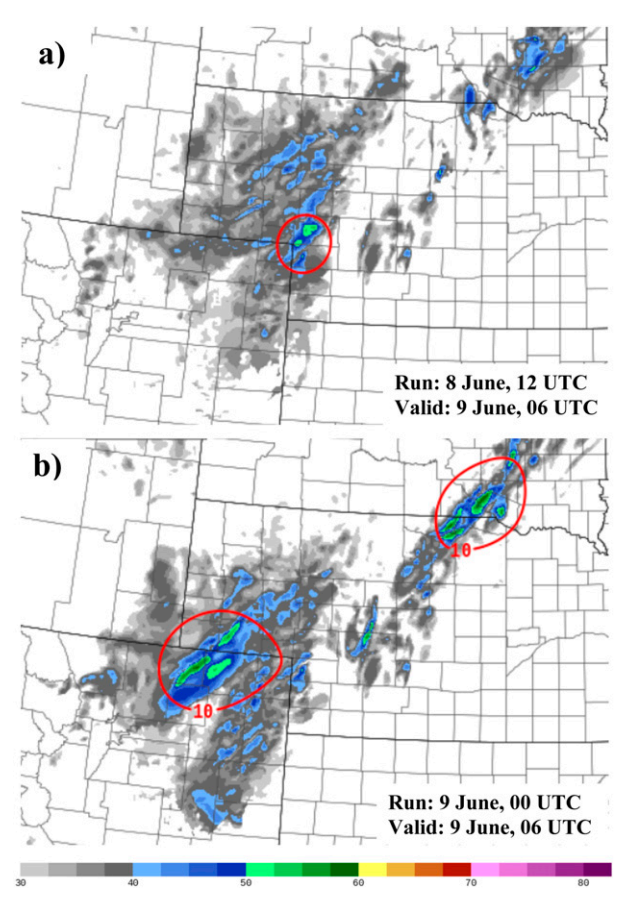


FIG. 16. HREF 4-h probability of 50-kt wind speeds (red contours) and ensemble maximum 10-m wind speed (shading) forecast where dBZ > 20 for the (a) 1200 UTC 8 Jun and (b) 0000 UTC 9 Jun forecasts valid 0600 UTC 9 Jun.

bearing some resemblance to the Akron macroburst storm are located near Akron and further north in Logan County, Colorado. The northern storm is stronger and has begun to leave a 20-m s⁻¹ wind swath in its wake.

A 6-h forecast sounding generated from the 4-km WRF simulation, valid at 0600 UTC for the grid point nearest KAKO (Fig. 18), looks quite similar in structure to the RAP proximity sounding at the same time (Fig. 6c). The atmosphere is nearly saturated between 750 and 500 hPa, and a stable layer exists between 725 and 700 hPa. One notable difference is the presence of a dry-adiabatic near-surface layer in the WRF sounding. Only the most unstable parcel, lifted from 668 hPa, has any CAPE (850 J kg $^{-1}$). As in the RAP soundings, there is a very sharp wind direction shift at the LCL of the most unstable parcel, with northwesterlies below and southerlies above, yielding 46.3 m s $^{-1}$ of 0–6-km vertical wind shear.

Despite the timing and spatial discrepancies between model forecasts and verification, the fact that gravity wave structures in convective cells were captured by convection-allowing models approximately 6 h in advance of a major macroburst event is remarkable. Moreover, the agreement of the model and analysis soundings and their overall resemblance to a

typical microburst profile are noteworthy. This case study thus lends evidence that convection-allowing models can provide meaningful forecast guidance for local misoscale and mesoscale high-impact events.

6. Discussion

The high-resolution observations of the Akron macroburst show some semblance to the conceptual model of microbursts put forward in seminal work by Fujita (1978, 1981) and Wakimoto (1982). Namely, relatively cool air existed at the surface following the passage of a cold front earlier in the day; an intense pressure surge was noted, in most cases immediately prior to the strongest downburst outflow wind gusts; and the damage pattern in Akron was indicative of both a strong southerly outflow boundary and rapidly shifting wind directions with radial outflow spreading out from the downburst epicenter. Whereas Wakimoto's (1982) conceptual model predicts a temperature drop as the downburst manifests at the surface, unique to the Akron case is a nontrivial temperature increase around the time of the most intense pressure surge. With the unprecedentedly high temporal resolution of the EC tower site, two additional temperature spikes are able to be observed several minutes later, which is likely due to mixing down relatively warmer air from the overlying inversion layer. It should be noted that the mechanism to produce heat bursts also involves a temperature spike in advance of strong winds reaching the surface, similar to what occurred here.

Given the fact that a positive surface pressure perturbation (i.e., high pressure) exists below a descending column of air as it decelerates and is deflected outward, surface pressure perturbations measured by the EC tower can be used to estimate the downdraft velocity v of the parent thunderstorm via a Bernoulli equation (Markowski and Richardson 2010):

$$p'_{\rm sfc} = \overline{\rho} \left(-\frac{v^2}{2} + \text{DCAPE} \right),$$
 (2)

where $p'_{\rm sfc}$ is the pressure perturbation at the surface beneath a downdraft, $\bar{\rho}$ is the mean air density between the surface and the height at which p' becomes small, and DCAPE is downdraft CAPE as defined earlier. The v^2 , $\bar{\rho}$, and DCAPE are measured ~2 km AGL, and the negative sign connotes a downward velocity. Solving for v from representative values of $p'_{\rm sfc} = 5 \, \rm hPa$, $\bar{\rho} = -1 \, \rm kg \, m^3$, and an estimated DCAPE = $800 \, \rm m^2 \, s^{-2}$ from SPC mesoanalysis, yields a downdraft velocity of 24.5 m s⁻¹. This value is slightly less than the radial outflow speeds observed, which are likely also influenced by the storm motion in excess of $13 \, \rm m \, s^{-1}$ and strong vertical wind shear.

The fact that 10-Hz frequency data from the USDA EC tower reveals multiple oscillations in both pressure and temperature on the order of seconds, and multiple observing stations captured temperature spikes several minutes before the maximum wind gusts, indicate the presence of an additional misoscale element aside from the macroburst radial outflow. While the purpose of this work has been to showcase the high-resolution observations, follow-up work will aim to investigate

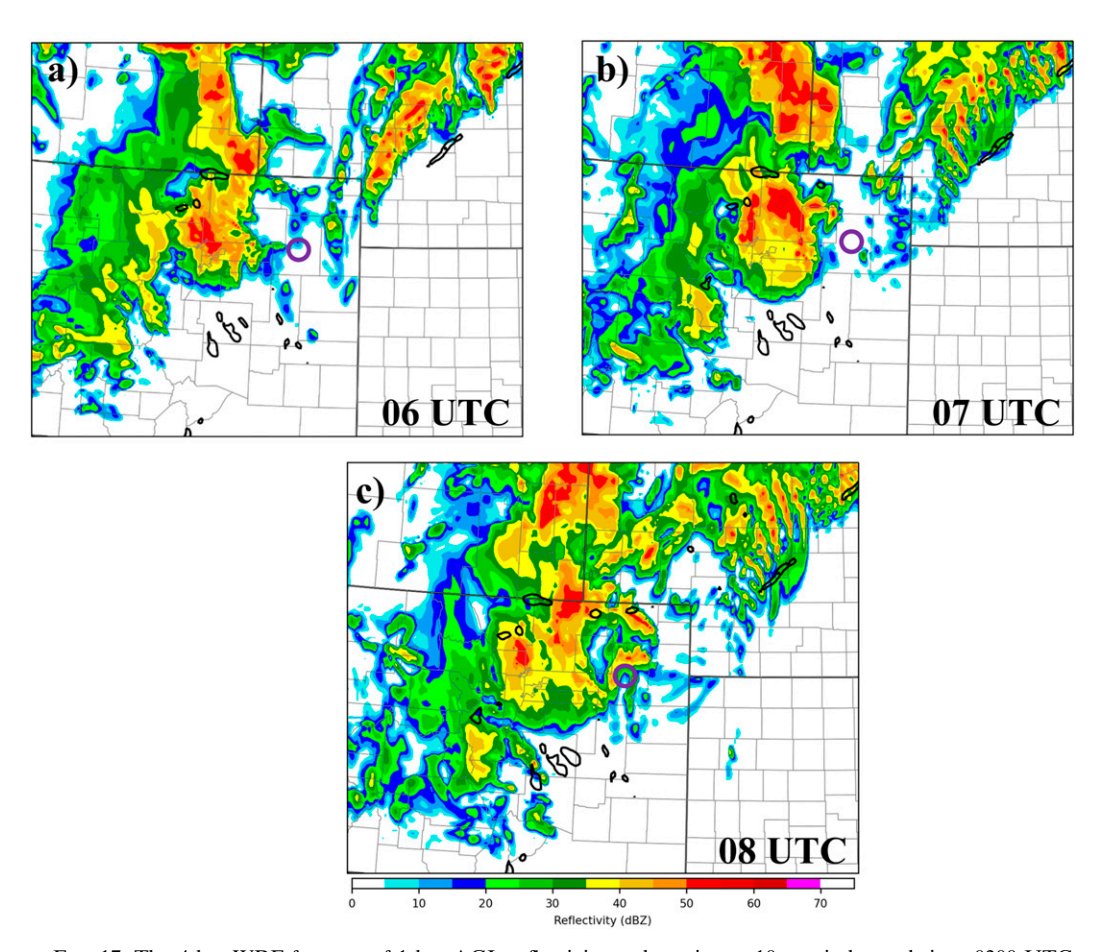


FIG. 17. The 4-km WRF forecast of 1-km-AGL reflectivity and maximum 10-m wind speed since 0300 UTC (contours represent wind swaths in excess $20 \,\mathrm{m\,s^{-1}}$), valid at (a) 0600, (b) 0700, and (c) 0800 UTC 9 Jun 2020. The simulation was initialized at 0000 UTC. Akron is represented by an open purple circle.

the small-scale wavelike features with the aid of nested highresolution models and develop a conceptual model of their interaction with the macroburst. Nevertheless, a few possibilities are worth postulating here. One possibility is a traveling microburst (Fujita 1981), with the downdraft winds reaching the surface and racing ahead of the region of precipitation and cold dome. This scenario could help to explain the spike and sudden drop in temperatures a few minutes ahead of and immediately following the maximum wind gusts, respectively, as was seen in the USDA tower and K2V6 data. Essentially an outflow boundary is created in this scenario, with temperatures rising before the boundary passes, and the dropping in its wake in the cold dome; however, the high pressure within the cold dome in Fujita's depiction of a traveling microburst is not seen in the observations, and the temperature increase predicted ahead of an outflow boundary should be more gradual than the sudden spike indicated in the observations. Hjelmfelt (1987) describes how some microburst outflows do not show a diverging radial pattern in all directions when manifesting within strong low-level background flow. Such was the case in and around Akron, with near-surface northerly winds around $15 \,\mathrm{m \, s^{-1}}$ in addition to strong southerly flow aloft.

A second possibility that could in fact be the same feature as Fujita's traveling microburst is that given the strong—and in some cases deep-stable layer sandwiched by two mixed layers (and a sharp decline in Scorer parameter), a bore or other gravity wave feature could have been trapped and traveling through the stable layer ahead of the macroburst, which served to mix warm air downward in its wake and cause a pressure surge ahead of its passage. The larger-scale pattern of convective fingers seen on this night is also consistent with trapped waves, and Rottman and Simpson (1989) note that some bores can have extensive mixing behind the head, followed by additional undulations, which is consistent with the observations here. The convective cell itself could have also created an outflow boundary that propagated northeastward, inducing a pressure spike and strong winds as air rode up and over it. Damage patterns in and around Akron also hint at multiple convective features, with some areas of treefall in opposite directions one block apart and other areas with damage consistent with a strong southwesterly storm outflow motion. The cell of interest was also elongating as it entered Akron, which could explain the eastward oriented damage seen south and west of Akron. The power of the high-

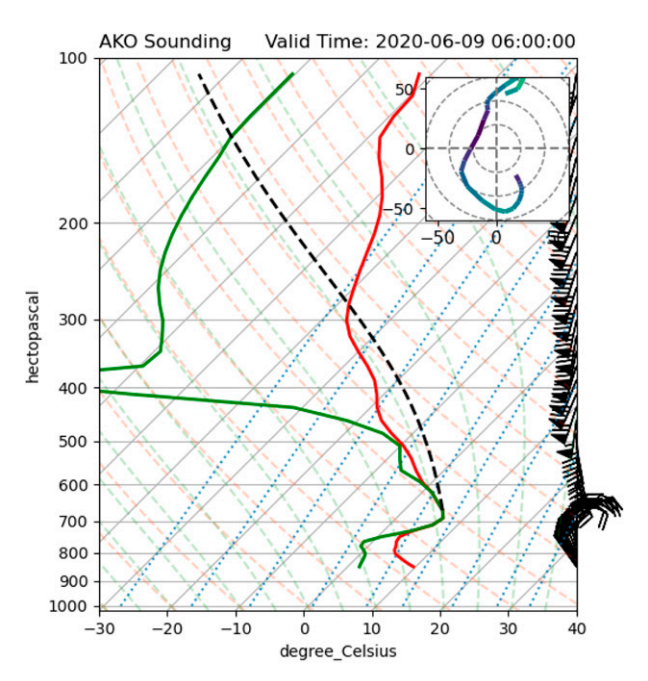


FIG. 18. Forecast sounding for AKO, initialized at 0000 UTC and effective at 0600 UTC, from a 4-km WRF simulation. Hodograph and wind barbs are in knots, where a flag represents 50 kt, a full barb is 10 kt, and a half barb is 5 kt.

frequency observations motivates simulations to explore these possibilities further and elucidate the complex mesoscale interactions on this night.

The Akron macroburst observations can also add to a growing body of work that highlights the importance of smallscale convective wind events on the development and vulnerability of wind engineering standards (Letchford et al. 2002; Lombardo et al. 2014). For example, Lombardo et al. (2014) exposed the idea of "ramp-up" wind events with time scales of abrupt wind speed increases on the order of a few minutes which is shorter than those used in many wind engineering applications. The Akron macroburst event showed an even more robust wind speed spike on the order of tens of seconds. Put alongside other small-scale severe wind events that have been analyzed at high temporal and/or spatial resolution (Orwig and Schroeder 2007; Gunter et al. 2017), the Akron macroburst can help inform wind load considerations within the engineering community for rapid-onset winds that pose different threats to infrastructure than more sustained synoptic high wind events.

7. Summary and application

The Akron macroburst of 9 June 2020 may well be the best observed of its kind, owing to the wealth of high-resolution data from a variety of weather stations across its path of impact. A 5-hPa pressure surge in 19 s immediately prior to the downdraft reaching the surface, a subsequent 15-hPa pressure drop following the radial outflow winds, an attendant temperature spike of up to 3°C as the macroburst occurred, and

extreme wind gusts in excess of 50 m s⁻¹ measured at multiple stations and different altitudes are unprecedented among downburst observations of recent decades.

The complex interplay of synoptic and mesoscale environments on this night precluded a more accurate forecast of downburst activity across northeastern Colorado. Multiple convection-allowing models hinted at a wavelike convective structure, and RAP soundings showed the presence of dry air aloft, elevated instability, and very strong vertical wind shear, an environment that provided a platform for air to acquire high levels of negative buoyancy and descend rapidly to the surface within the convection. However, surface air was relatively cold and the low-level environment highly stable with a strong temperature inversion in the post-cold-frontal air mass, a nonideal scenario for downbursts. The Akron storm is unique for its sudden intensification eastward as it moved north, whereas at least nine other "fingers" of convection noted on this night across northeastern Colorado and Nebraska were oriented north-south. Storms generally moved north or northeastward, driven by the upper-level steering flow but opposing low-level northerlies, creating an environment of rich vertical wind shear $> 45 \,\mathrm{m\,s^{-1}}$. Proximity soundings show the evolution of a low-level moist layer and temperature inversion, with a dry layer aloft, characteristics of typical wet microburst soundings (Atkins and Wakimoto 1991).

While the USDA towers were able to record the macroburst event at incredibly high temporal resolution, nearby stations in Akron and other towns also show similar progressions of temperature, pressure, and winds on this night. The presence of this relatively dense array of weather observing stations within networks such as CWOP, CoAgMet, and MesoWest allowed for the verification of the high wind speeds as well as the validity of the temperature and pressure undulations, which were captured at various temporal resolutions. Moreover, the first and third highest thunderstorm wind gusts in Colorado state history were recorded during this event from local weather stations. The fact that observations were consistent across various platforms and instrumentation gives us both confidence and intrigue to pursue a more detailed modeling analysis of this event. These high-resolution observations, therefore, can motivate local program managers toward valuing and maintaining local weather stations, as their functionality has proven here to be of great worth in contributing to a research area that has been relatively scant in recent years.

While this work has presented an observational perspective on the severe Akron macroburst, questions remain as to how high-resolution convection-allowing models can simulate and forecast the unique elements of the case. Of interest is to investigate and quantify the apparent gravity wave and/or bore features that accompanied the severe downburst winds. As such, future work will use idealized simulations initialized with a representative sounding from Akron to determine how this specific environment amplified thunderstorm downdrafts to such intense levels. Such investigation will increase understanding of downbursts and help aid in forecasting such events. Moreover, the quality and quantity of the Akron macroburst observations serve as a valuable source of information that can be leveraged by the forecasting and research communities to

better understand the wind, pressure, and temperature oscillations associated with these events. The Akron macroburst has also raised awareness of downburst events in the High Plains, and highlights both the challenge of and need for effective risk communication of downburst potential in a place like eastern Colorado, where downbursts are relatively common but rarely affect population areas and are not given as much attention as hailstorms and tornadoes. The hope is that the observations presented here, coupled with future modeling analysis and additional case studies, can aid in improved understanding of downbursts and the development of useful short-term forecasts for these rapid-onset severe wind events.

Acknowledgments. Data from the 10-m and EC towers at the USDA site belong to and used with permission by David Poss with USDA and John Tatarko of the Rangeland Resources and Systems Unit in Fort Collins. Greg Hanson from the NWS forecast office in Boulder provided photos and information from the storm survey that was conducted after the macroburst. The authors are also thankful for the CWOP station owner for his insights on his weather station setup, and Stacey Hitchcock for providing feedback on initial data analysis and motivation for a follow-up modeling study. Radar images in Fig. 4 were generated using Py-art (Helmus and Collis 2016), and Figs. 3, 5, 6, and 18 were generated using MetPy (May et al. 2020). This work was supported by the National Science Foundation (NSF) Grants AGS-1636663 and AGS-1636667 as well as the USDA National Institute of Food and Agriculture and Colorado Agricultural Experiment Station Project COL00703B.

Data availability statement. Observational data can be accessed online for ASOS (https://synopticdata.com/) and CoAgMET (https://coagmet.colostate.edu/) stations. CWOP and USDA data are available upon permission from the respective owners and request from the authors. HREF model forecasts were taken from the SPC HREF ensemble viewer, available at https://www.spc.noaa.gov/exper/href/?model=href&product=cref_members§or=cp&rd=0000. Atmospheric soundings were generated from the University of Wyoming archive (http://weather.uwyo.edu/upperair/sounding.html) and the RAP archive (https://www.ncdc.noaa.gov/data-access/model-data/model-datasets/rapid-refresh-rap). The CSU 4-km WRF configuration and data are available upon request.

REFERENCES

- Adams-Selin, R. D., 2020a: Impact of convectively generated low-frequency gravity waves on evolution of mesoscale convective systems. J. Atmos. Sci., 77, 3441–3460, https://doi.org/10.1175/JAS-D-19-0250.1.
- ——, 2020b: Sensitivity of MCS low-frequency gravity waves to microphysical variations. *J. Atmos. Sci.*, 77, 3461–3477, https:// doi.org/10.1175/JAS-D-19-0347.1.
- —, and R. H. Johnson, 2013: Examination of gravity waves associated with the 13 March 2003 bow echo. *Mon. Wea. Rev.*, **141**, 3735–3756, https://doi.org/10.1175/MWR-D-12-00343.1.
- Atkins, N. T., and R. M. Wakimoto, 1991: Wet microburst activity over the southeastern United States: Implications for forecasting. *Wea. Forecasting*, **6**, 470–482, https://doi.org/10.1175/1520-0434(1991)006<0470:WMAOTS>2.0.CO;2.

- Benjamin, S. G., and Coauthors, 2016: A North American hourly assimilation and model forecast cycle: The Rapid Refresh. *Mon. Wea. Rev.*, 144, 1669–1694, https://doi.org/10.1175/ MWR-D-15-0242.1.
- Biernat, K. A., and L. Orf, 2014: Analysis of wet and dry microburst simulations and the importance of the elevated dry layer on wet microburst formation and strength. *13th Annual Student Conf.*, Atlanta, GA, Amer. Meteor. Soc., S4, https://ams.confex.com/ams/94Annual/webprogram/Paper242382.html.
- Bolgiani, P., S. Fernández-González, F. Valero, A. Merino, E. García-Ortega, J. L. Sánchez, and M. L. Martín, 2020: Simulation of atmospheric microbursts using a numerical mesoscale model at high spatiotemporal resolution. *J. Geophys. Res. Atmos.*, **125**, e2019JD031791, https://doi.org/10.1029/2019JD031791.
- Burlando, M., D. Romanić, G. Solari, H. Hangan, and S. Zhang, 2017: Field data analysis and weather scenario of a downburst event in Livorno, Italy, on 1 October 2012. Mon. Wea. Rev., 145, 3507–3527, https://doi.org/10.1175/MWR-D-17-0018.1.
- Chasteen, M. B., S. E. Koch, and D. B. Parsons, 2019: Multiscale processes enabling the longevity and daytime persistence of a nocturnal mesoscale convective system. *Mon. Wea. Rev.*, 147, 733–761, https://doi.org/10.1175/MWR-D-18-0233.1.
- Childs, S. J., R. S. Schumacher, and S. M. Strader, 2020: Projecting end-of-century human exposure from Tornadoes and severe hailstorms in Eastern Colorado: Meteorological and population perspectives. Wea. Climate Soc., 12, 575–595, https:// doi.org/10.1175/WCAS-D-19-0153.1.
- Clark, M. R., J. D. Webb, and P. J. Kirk, 2018: Fine-scale analysis of a severe hailstorm using crowd-sourced and conventional observations. *Meteor. Appl.*, 25, 472–492, https://doi.org/ 10.1002/met.1715.
- Coleman, T. A., and K. R. Knupp, 2011: Radiometer and profiler analysis of the effects of a bore and a solitary wave on the stability of the nocturnal boundary layer. *Mon. Wea. Rev.*, 139, 211–223, https://doi.org/10.1175/2010MWR3376.1.
- —, —, and D. Herzmann, 2009: The spectacular undular bore in Iowa on 2 October 2007. *Mon. Wea. Rev.*, **137**, 495–503, https://doi.org/10.1175/2008MWR2518.1.
- Creager, G. J., R. Chadwick, D. Helms, P. A. Miller, M. F. Barth, P. Gladstone, and S. S. Dimse, 2009: Observing the urban mesoscale environment: The Citizen Weather Observing Program. *Eighth Symp. on the Urban Environment*, Phoenix, AZ, Amer. Meteor. Soc., JP1.7, https://ams.confex.com/ams/ 89annual/techprogram/paper_150514.htm.
- Davis, C., and Coauthors, 2004: The Bow Echo and MCV Experiment: Observations and opportunities. *Bull. Amer. Meteor. Soc.*, 85, 1075–1094, https://doi.org/10.1175/BAMS-85-8-1075.
- Doesken, N. J., H. R. Duke, B. L. Hamblen, J. Kleist, T. B. McKee, M. S. McMillan, and H. F. Schwartz, 1998: The Colorado Agricultural Meteorological Network (CoAgMet)—A unique collaborative system supporting Colorado agriculture. 23rd Conf. on Agriculture and Forest Meteorology, Albuquerque, NM, Amer. Meteor. Soc., 240–242.
- Doswell, C. A. III, H. E. Brooks, and M. P. Kay, 2005: Climatological estimates of daily local nontornadic severe thunderstorm probability for the United States. Wea. Forecasting, 20, 577–595, https:// doi.org/10.1175/WAF866.1.
- Edwards, R., J. T. Allen, and G. W. Carbin, 2018: Reliability and climatological impacts of convective wind estimations. *J. Appl. Meteor. Climatol.*, 57, 1825–1845, https://doi.org/10.1175/ JAMC-D-17-0306.1.

- Forbes, G. S., and R. M. Wakimoto, 1983: A concentrated outbreak of tornadoes, downbursts and microbursts, and implications regarding vortex classification. *Mon. Wea. Rev.*, **111**, 220–236, https://doi.org/10.1175/1520-0493(1983)111<0220:ACOOTD> 2.0.CO:2.
- Fujita, T. T., 1978: Manual of downburst identification for Project NIMROD. SMRP Research Paper 156, University of Chicago, 104 pp. [NTIS PB-286048].
- ——, 1981: Tornadoes and downbursts in the context of generalized planetary scales. J. Atmos. Sci., 38, 1511–1534, https://doi.org/ 10.1175/1520-0469(1981)038<1511:TADITC>2.0.CO;2.
- —, 1985: The downburst: Microburst and macroburst. SMRP Research Paper 210, University of Chicago, 122 pp. [NTIS PB85-148880].
- ——, 1990: Downbursts: Meteorological features and wind field characteristics. J. Wind Eng. Ind. Aerodyn., 36, 75–86, https:// doi.org/10.1016/0167-6105(90)90294-M.
- Gilmore, M. S., and L. J. Wicker, 1998: The influence of midtropospheric dryness on supercell morphology and evolution. *Mon. Wea. Rev.*, 126, 943–958, https://doi.org/10.1175/1520-0493(1998)126<0943:TIOMDO>2.0.CO;2.
- Gultepe, I., and Coauthors, 2019: A review of high impact weather for aviation meteorology. *Pure Appl. Geophys.*, **176**, 1869– 1921, https://doi.org/10.1007/s00024-019-02168-6.
- Gunter, W. S., J. L. Schroeder, C. C. Weiss, and E. C. Bruning, 2017: Surface measurements of the 5 June 2013 damaging thunderstorm wind event near Pep, Texas. *Wind Struct.*, 24, 185–204, https://doi.org/10.12989/was.2017.24.2.185.
- Haertel, P. T., R. H. Johnson, and S. N. Tulich, 2001: Some simple simulations of thunderstorm outflows. *J. Atmos. Sci.*, **58**, 504–516, https://doi.org/10.1175/1520-0469(2001)058<0504: SSSOTO>2.0.CO:2.
- Helmus, J., and S. Collis, 2016: The Python ARM Radar Toolkit (Py-ART), a library for working with weather radar data in the Python programming language. *J. Open Res. Software*, **4**, e25, https://doi.org/10.5334/jors.119.
- Hjelmfelt, M. R., 1987: The microbursts of 22 June 1982 in JAWS. J. Atmos. Sci., 44, 1646–1665, https://doi.org/10.1175/1520-0469(1987)044<1646:TMOJIJ>2.0.CO:2.
- ——, 2010: Microbursts and macrobursts: Windstorms and blowdowns. *Plant Disturbance Ecology: The Process and the Response*, E. Johnson and K. Miyanishi, Eds., Academic Press, 59–101.
- Järvi, L., and Coauthors, 2007: Micrometeorological observations of a microburst in southern Finland. *Bound.-Layer Meteor.*, 125, 343–359, https://doi.org/10.1007/s10546-007-9204-7.
- Johnson, R. H., 2001: Surface mesohighs and mesolows. Bull. Amer. Meteor. Soc., 82, 13–31, https://doi.org/10.1175/1520-0477(2001)082<0013:SMAM>2.3.CO;2.
- Klemp, J. B., 1987: Dynamics of tornadic thunderstorms. *Annu. Rev. Fluid Mech.*, **19**, 369–402, https://doi.org/10.1146/annurev.fl.19.010187.002101.
- Koch, S. E., P. B. Dorian, R. Ferrare, S. H. Melfi, W. C. Skillman, and D. Whiteman, 1991: Structure of an internal bore and dissipating gravity current as revealed by Raman lidar. *Mon. Wea. Rev.*, 119, 857–887, https://doi.org/10.1175/1520-0493(1991) 119<0857:SOAIBA>2.0.CO;2.
- Letchford, C. W., C. Mans, and M. T. Chay, 2002: Thunderstorms— Their importance in wind engineering (a case for the next generation wind tunnel). *J. Wind Eng. Ind. Aerodyn.*, **90**, 1415–1433, https://doi.org/10.1016/S0167-6105(02)00262-3.
- Lin, W. E., L. G. Orf, E. Savory, and C. Novacco, 2007: Proposed large-scale modelling of the transient features of a downburst

- outflow. Wind Struct., 10, 315–346, https://doi.org/10.12989/was.2007.10.4.315.
- Lombardo, F. T., D. A. Smith, J. L. Schroeder, and K. C. Mehta, 2014: Thunderstorm characteristics of importance to wind engineering. *J. Wind Eng. Ind. Aerodyn.*, 125, 121–132, https:// doi.org/10.1016/j.jweia.2013.12.004.
- Markowski, P., and Y. Richardson, 2010: Mesoscale Meteorology in Midlatitudes. Wiley-Blackwell, 430 pp.
- Marsham, J. H., S. B. Trier, T. M. Weckwerth, and J. W. Wilson, 2011: Observations of elevated convection initiation leading to a surface-based squall line during 13 June IHOP_2002. *Mon. Wea. Rev.*, 139, 247–271, https://doi.org/10.1175/ 2010MWR3422.1.
- May, R. M., S. C. Arms, P. Marsh, E. Bruning, J. R. Leeman, K. Goebbert, J. E. Thielen, and Z. Bruick, 2020: MetPy: A Python package for meteorological data. Unidata, accessed 14 October 2020, https://github.com/Unidata/MetPy.
- McCarthy, J., J. W. Wilson, and T. T. Fujita, 1982: The joint airport weather studies project. *Bull. Amer. Meteor. Soc.*, **63**, 15–22, https://doi.org/10.1175/1520-0477(1982)063<0015: TJAWSP>2.0.CO:2.
- Metz, N. D., and L. F. Bosart, 2010: Derecho and MCS development, evolution, and multiscale interactions during 3–5 July 2003. Mon. Wea. Rev., 138, 3048–3070, https://doi.org/10.1175/2010MWR3218.1.
- Mueller, D., B. Geerts, Z. Wang, M. Deng, and C. Grasmick, 2017: Evolution and vertical structure of an undular bore observed on 20 June 2015 during PECAN. *Mon. Wea. Rev.*, **145**, 3775–3794, https://doi.org/10.1175/MWR-D-16-0305.1.
- National Weather Service, 2020: June 8–9 2020 macroburst, high wind, and mountain snow. NOAA/NWS, Boulder, CO, accessed 15 September 2020, https://www.weather.gov/bou/20200609Macroburst.
- NSSL, 2020: Severe Weather 101: Types of damaging winds. National Severe Storms Laboratory, accessed 8 September 2020, https://www.nssl.noaa.gov/education/svrwx101/wind/types/.
- Oreskovic, C., L. G. Orf, and E. Savory, 2018: A parametric study of downbursts using a full-scale cooling source model. *J. Wind Eng. Ind. Aerodyn.*, **180**, 168–181, https://doi.org/10.1016/j.jweia.2018.07.020.
- Orf, L., E. Kantor, and E. Savory, 2012: Simulation of a downburst-producing thunderstorm using a very high-resolution three-dimensional cloud model. *J. Wind Eng. Ind. Aerodyn.*, **104–106**, 547–557, https://doi.org/10.1016/j.jweia.2012.02.020.
- Orwig, K. D., and J. L. Schroeder, 2007: Near-surface wind characteristics of extreme thunderstorm outflows. J. Wind Eng. Ind. Aerodyn., 95, 565–584, https://doi.org/10.1016/j.jweia. 2006.12.002.
- Proctor, F. H., 1988: Numerical simulations of an isolated microburst. Part I: Dynamics and structure. J. Atmos. Sci., 45, 3137–3160, https://doi.org/10.1175/1520-0469(1988)045<3137: NSOAIM>2.0.CO;2.
- Roberts, B., B. T. Gallo, I. L. Jirak, and A. J. Clark, 2019: The High Resolution Ensemble Forecast (HREF) system: Applications and performance for forecasting convective storms. 2019 AGU Fall Meeting, San Francisco, CA, Amer. Geophys. Union, Abstract A31O-2797.
- Rottman, J. W., and J. E. Simpson, 1989: The formation of internal bores in the atmosphere: A laboratory model. *Quart. J. Roy. Meteor. Soc.*, **115**, 941–963, https://doi.org/10.1002/qj.49711548809.
- Rotunno, R., and J. B. Klemp, 1982: The influence of the shear-induced pressure gradient on thunderstorm motion. *Mon.*

- Wea. Rev., 110, 136–151, https://doi.org/10.1175/1520-0493(1982) 110<0136:TIOTSI>2.0.CO;2.
- Schumacher, R. S., 2015: Resolution dependence of initiation and upscale growth of deep convection in convection-allowing forecasts of the 31 May–1 June 2013 supercell and MCS. *Mon. Wea. Rev.*, 143, 4331–4354, https://doi.org/10.1175/MWR-D-15-0179.1.
- ——, 2020: What is a derecho? An atmospheric scientist explains these rare but dangerous storm systems. *The Conversation*, 15 June 2020, https://theconversation.com/what-is-a-derechoan-atmospheric-scientist-explains-these-rare-but-dangerousstorm-systems-140319.
- Sedgwick County Office of Emergency Manager, 2020: Preliminary damage assessment, June 9th, 2020. Sedgwick County, KS.
- Shreffler, J. H., and F. S. Binkowski, 1981: Observations of pressure jump lines in the Midwest, 10–12 August 1976. *Mon. Wea. Rev.*, **109**, 1713–1725, https://doi.org/10.1175/1520-0493(1981) 109<1713:OOPJLI>2.0.CO;2.
- van Dijke, D., Y. Hinssen, and F. Bijlsma, 2011: A 500m WRF hindcast of a microburst event in The Netherlands. European

- Meteorological Society Annual Meeting, Berlin, Germany, European Meteorological Society, Abstract EMS2011-546-1, Vol. 8, 1–4.
- Vermeire, B. C., L. G. Orf, and E. Savory, 2011: Improved modelling of downburst outflows for wind engineering applications using a cooling source approach. *J. Wind Eng. Ind. Aerodyn.*, **99**, 801–814, https://doi.org/10.1016/j.jweia.2011.03.003.
- Wakimoto, R. M., 1982: The life cycle of thunderstorm gust fronts as viewed with Doppler radar and rawinsonde data. *Mon. Wea. Rev.*, **110**, 1060–1082, https://doi.org/10.1175/1520-0493(1982)110<1060:TLCOTG>2.0.CO;2.
- ——, 1985: Forecasting dry microburst activity over the high plains. *Mon. Wea. Rev.*, **113**, 1131–1143, https://doi.org/10.1175/1520-0493(1985)113<1131:FDMAOT>2.0.CO;2.
- —, and V. N. Bringi, 1988: Dual-polarization observations of microbursts associated with intense convection: The 20 July storm during the MIST project. *Mon. Wea. Rev.*, 116, 1521–1539, https://doi.org/10.1175/1520-0493(1988) 116<1521:DPOOMA>2.0.CO;2.